International Journal of Nanomedicine

Dovepress
open access to scientific and medical research

Open Access Full Text Article

REVIEW

Nanotechnology, from quantum mechanical calculations up to drug delivery

This article was published in the following Dove Press journal:
International Journal of Nanomedicine

Beata Szefler

Department of Physical Chemistry, Faculty of Pharmacy, Collegium Medicum, Nicolaus Copernicus University, Bydgoszcz, Poland

Abstract: There are several reasons why nanotechnology is currently considered as the leader among the most intensively developing research trends. Nanomatter often exhibits new properties, other than those of the morphology of a continuous solid. Also, new phenomena appear at the nanoscale, which are unknown in the case of microcrystalline objects. For this reason, nanomaterials have already found numerous applications that are described in this review. However, among intensively developed various branches of nanotechnology, nanomedicine and pharmacology stand out particularly, which opens new possibilities for the development of these disciplines, gives great hope for the creation of new drugs in which toxicological properties are reduced to a minimum, reduces the doses of medicines, offers targeted treatment and increases diagnostic possibilities. Nanotechnology is the source of a great revolution in medicine. It gives great hope for better and faster treatment of many diseases and gives hope for a better tomorrow. However, the creation of new "nanodrugs" requires a special understanding of the properties of nanoparticles. This article is a review work which determines and describes the way of creating new nanodrugs from ab initio calculations by docking and molecular dynamic applications up to a new medicinal product, as a proposal for the personalized medicine, in the early future.

Keywords: fullerenes, nanoparticles, drug delivery, personalized medicine, ab initio, molecular dynamics

Introduction

In the last quarter of the century, fullerenes became one of the dominant discoveries in the field of physical chemistry. Fullerenes are a new allotropic form of carbon. Research on them has contributed to a huge number of scientific publications and their use is restricted by several hundred patents. In the year 1996, three explorers, Harold Kroto, Richard Smalley and Robert Curl, received the Nobel Prize in this field of chemistry, which confirmed the importance of this kind of science.[1] Not so long ago, it was thought that coal occurs in two allotropic forms that differ in their crystal structure, namely, diamond and graphite, but in 1985, the above-mentioned scientists revolutionized knowledge about carbon and discovered a new allotropic variety, a caged form of carbon.[2] The crystal structure of fullerenes is completely different from graphite and diamond, since it is made up of C_{60} and C_{70} carbon molecules. There are two fundamental differences between graphite, diamond and fullerenes. The first two mentioned varieties of carbon occur in atomic form, while fullerenes are its molecular form. In the crystalline networks of diamond or graphite, peripheral atoms are saturated with other elements, most often more reactive hydrogen; so, formally, carbon in these varieties does not occur in pure form. Fullerenes, on the

Correspondence: Beata Szefler
Department of Physical Chemistry, Faculty of Pharmacy, Collegium Medicum, Nicolaus Copernicus University, Kurpińskiego 5, 85-096 Bydgoszcz, Poland
Email beatas@cm.umk.pl

submit your manuscript | www.dovepress.com
Dovepress
http://dx.doi.org/10.2147/IJN.S172907

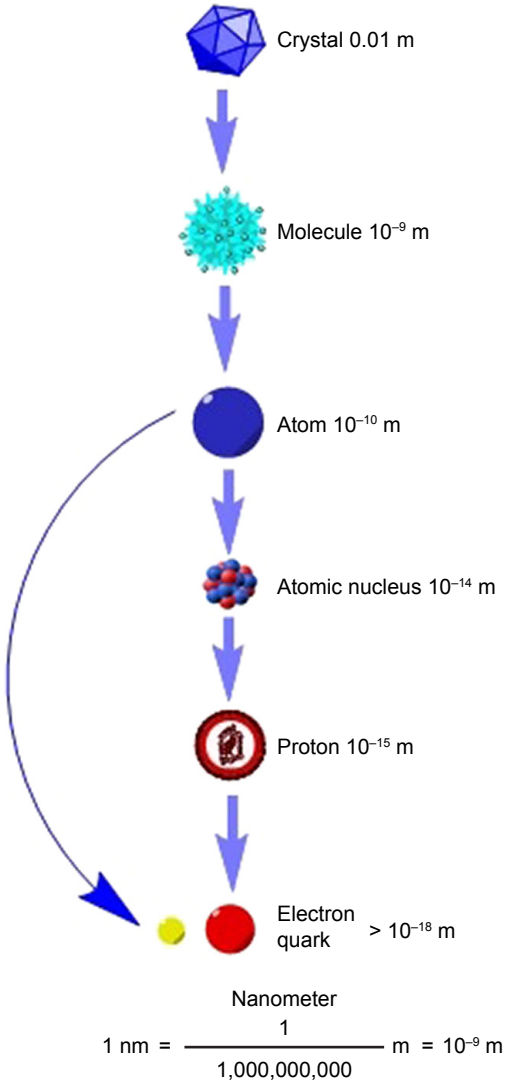

Figure 1 How small is the nanometer?

other hand, are a variety of pure carbon. The discovery of fullerenes and the enormous development of research in this field have led to increased knowledge about carbon nanostructures. At the beginning of the 90s, carbon nanotubes (CNTs), carbon nanocrystallites with onion structure and carbon nanocapsules were discovered. Nanotechnology is an absolutely new quality in technology and, at the same time, it is something so different that it cannot be compared to anything else. It is an action in the world of small objects with sizes reaching individual molecules of chemical compounds. The smallest objects which man had dealt with were located on a micro-scale, which means that they were described in millionth of a meter. This was practically enough to deal with the anatomical description of the cells of living organisms and some of their structural parts. A limitation of the study of smaller structures was the resolution of optical microscopes. After the invention of the electron microscope in 1931, it became possible to distinguish two separate points even closer together. Nanotechnology can be defined as a science dealing with objects for which the smallest elementary particle does not exceed 100 nm even in one plane (Figure 1). This size is, in fact, comparable with the size of macromolecules such as enzymes or receptors (about 5 nm) and is smaller than the human cell, whose size is estimated at 10,000–20,000 nm.[3–5]

This technology interferes with the structure of matter at the molecular level, and thanks to this, we can count on the rapid development of certain fields of science, particularly material engineering, as well as chemistry, electronics, optics, pharmacy, medicine and cosmetology. Thanks to nanostructures, many physicochemical properties of substances, for example, melting point and color, can be controlled.

Structure

Fullerenes are (besides graphite and diamond) the third allotropic form of carbon. This name covers the entire family of molecules with the general formula C2n (n>16), in which the surface of the solid is built of only carbon atoms, located only on its surface (Figure 2).

Among the large fullerene family, fullerenes containing 60 or 70 carbon atoms are the most widespread (Figure 3) and, at the same time, the best-known ones.[3,6,7] Studies of carbon clusters by mass spectrometry show that the "carbon ball family" is almost infinitely large. The knowledge of higher fullerenes is quite limited due to their much lower availability. The most popular fullerene (Figure 3), containing 60 carbon atoms (the Buckminster fullerene C_{60}), has the shape of a truncated icosahedron, that is, it looks exactly like a football. C_{70}, on the other hand, has an additional ring of carbon atoms and it is the best-known higher fullerene. Compared to C_{60}, its molecule has a hexagonal ring band attached to the middle, which reduces the symmetry of the fullerene cage. C_{70} has an ovoidal structure and has physicochemical properties similar to C_{60}.

These particles have many interesting qualities, and their electrochemical properties (Figure 4) are particularly interesting and intensely studied.[8–20]

Due to its spatial structure, the fullerene molecule C_{60} enjoys the greatest attention from scientists and it is considered to be an "ideal" structure (Figures 4 and 5). The C_{60} fullerene molecule has the shape of a spheroid, or more precisely a truncated icosahedron, which has

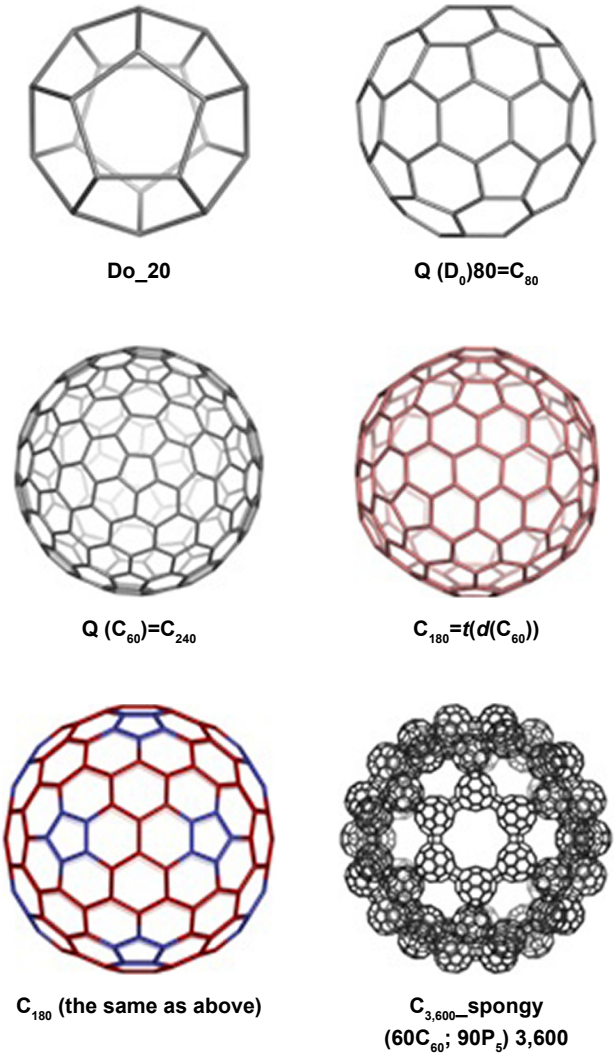

Figure 2 Fullerenes and a hyper-fullerene (bottom right corner).

60 vertices, each constituting one carbon atom (Figure 5). According to the theoretical proof of L Euler,[224] a symmetrical solid with C20+2n vertices must be enclosed by 12 pentagons and n hexagons. The smallest carbon cluster that meets this rule is C_{60} and its particles have a diameter slightly greater than 1 nm. Each of the C_{60} fullerene carbon atoms is surrounded by an identical environment; therefore, all atoms are equal and the molecule does not contain weak points of chemical interactions. Although the wrapping of the graphite layer in the carbon cage is accompanied by stresses, thanks to symmetry, they are distributed evenly across the molecule.[22] C_{60} molecules have a symmetrical structure and, thanks to that, they are extremely durable.[23]

Fullerenes classification

The multi-atom carbon fullerenes are completely empty inside and have a sufficiently large inner diameter to accommodate even the largest atoms of chemical elements (Figure 6), including radioactive elements and noble gas atoms (endohedral fullerenes).[24–26] Exohedral fullerenes, on the other hand, are fullerenes to which foreign atoms are joined from the outside of the fullerene cage. Heterofullerenes are fullerenes in which the carbon atoms are replaced by other atoms (Figure 7).

The results of research on the synthesis of endohedral fullerenes with uranium proved to be a surprise. The formation of a stable U @ C_{28} structure was proved, and also, model calculations showed that $C_{28}H_4$ fullerene having four external hydrogen atoms should be a very stable structure. Thus, the search for the smallest fullerene that can bind some chemical outside or inside the atoms of its cage seems to be an extremely important task.

The creation of new nano-objects requires a special understanding of the properties of nanoparticles, and because the carbon allotropy has a dominant role in nano-domain, both for theoretical reasons and their further applications, zero-, one-, two- and three-dimensional carbon-based structures were studied, such as fullerenes, nanotubes, graphene, spongy carbon and hyper-diamonds. As nano-structured functional materials, inorganic compounds such as silicates,

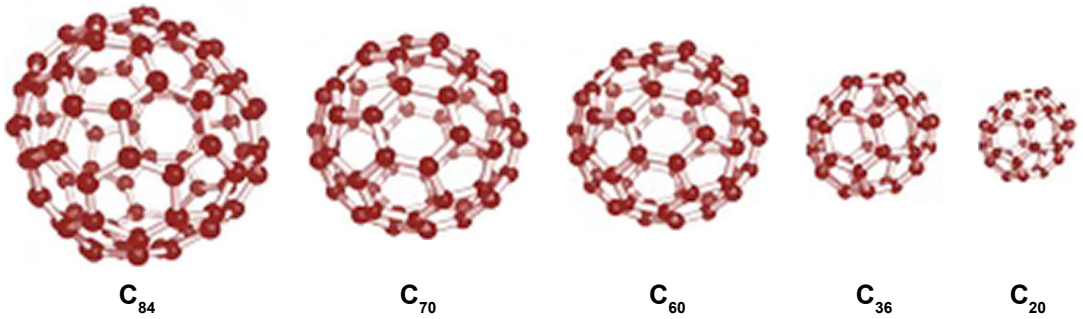

Figure 3 The most popular fullerenes.

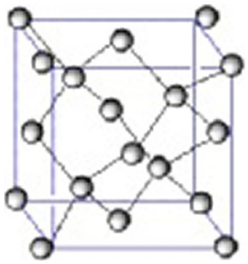

Diamond

Density: 3.47–3.56 g/cm^3

Color: White, yellow, red, green, blue, brown

Transparency: Transparent

Electrical conductivity: Insulator

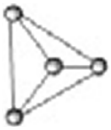

Thermal conductivity: Very good

Hardness: The hardest material

Graphite

Density: 2.25 g/cm^3

Color: Steel-gray

Electrical conductivity: Conducts electricity

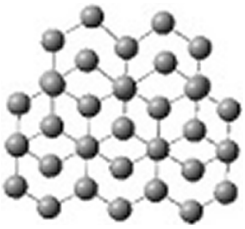

Thermal conductivity: Conducts heat

Hardness: Very soft

C–C bond length: 0.142 nm

Figure 4 Allotropic varieties of carbon.
Note: Data from Dubois et al.[21]

borates, selenides, sulfides and oxides have also found several applications. Action at the molecular level has led to the development of nanotechnology in many areas such as material engineering, chemistry, biology and cosmetic area, but in pharmacology and medicine, and quantum computing, it can be useful in providing the theoretical background for new syntheses and applications. Properties of fullerenes result mainly from their aromatic character.

Physicochemical properties of fullerenes

Fullerenes exhibit several similar general physicochemical properties. They do not dissolve well in typical organic solvents (much better in aromatic than in aliphatic ones), and the best solvents include benzene and its derivatives, toluene and carbon disulfide. Maximum solubility at 280 K does not increase with increasing temperature. The solution of C_{60} in toluene is purple and C_{70} is red. Fullerenes are easily solvated/combined with solvent molecules to form stable complexes. C_{60} molecules form a crystalline structure and their geometric structure corresponds to beveled regular icosahedron and has 12 pentagonal rings, 20 hexagonal rings and 30 double bonds located in six-membered rings. Fulleryte with a density of 1.65 g/cm^3 has the distance between centers equal to 1,004 nm and it is an electrical insulator. Despite the initially expected chemical inactivity of C_{60} and its derivatives, it turned out that fullerenes can be functionalized. Based on the way of functionalization, it was distinguished into exo- and endohedral forms of fullerenes and heterofullerenes.

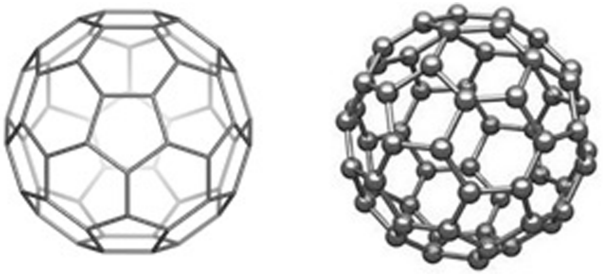

Figure 5 Spatial structure of the fullerene molecule C_{60}.

C_{60} and its homologues have interesting and often unique properties; hence, they show potential applications in many areas such as superconductivity, photo-optics, biochemistry, catalysis, material and fuel engineering. The physicochemical properties used in the areas of prospective application of fullerenes are illustrated in Figure 8:

In the 90s, CNTs, carbon nanocrystallites with "onion" structure and carbon nanocapsules were discovered.

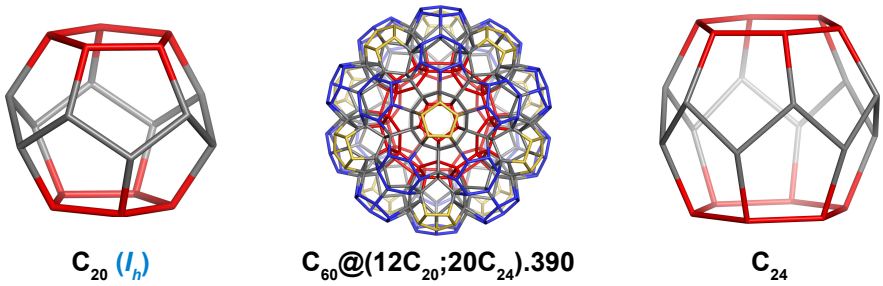

Figure 6 Examples of small and large fullerenes.
Note: Data from Jones[23] and Guo et al.[27]

Nanotubes are single-walled or multi-walled carbon tubes with a diameter of even <1 nm and lengths larger by many orders of magnitude with extremely interesting physicochemical properties.

The development of research in this field preceded by the discovery of fullerenes had resulted in tremendous increase in knowledge about the carbon nanostructure.

Chemical properties (aromaticity)

Fullerenes and other nanoparticles are aromatic structures. Aromaticity is used to describe the durability and reactivity of structures containing delocalized π electrons.[28–33] However, the delocalization of π electrons alone does not justify the particular durability that aromatic compounds have. The π electron cloud must contain a certain number of electrons, fulfilling the Hückel rule. The cyclic (planar) π electron system with (4n+2) electrons is more stable than the system containing (4n) electrons. Aromaticity is a multidimensional concept. Due to the complexity of the phenomenon of aromaticity, one parameter is not enough to describe it. The statistical surveys conducted show that two or even three independent indices are necessary to describe the variability of the aromatic character, hence the diversity of indexes describing the aromaticity of compounds.

In the "energetic criterion",[34–37] the concept of energy criterion is based on resonance energy and aromatic stabilization energy. This concept results from Pauling's theory of valence bonds. One of the effects of π electron delocalization is to increase the thermodynamic durability of molecules compared to similar structures in which such delocalization is not possible. However, in the case of nanoparticles, their stability and reactivity is related not only to the energy criterion, but also, above all, to their deformation.

In the "electronic criterion",[34,35,38] the distribution of π electron can be represented by the numerical structures of the Kekulé values, allowing the construction of one numerical structure to superimpose the geometric structures of Kekulé. An example may be icosahedral C_{60} which has 12,500 such structures. The higher the Kekulé structure, the higher is the stability.

Schleyer proved that the aromatic compounds are those structures that exhibit high magnetic susceptibility, "magnetic criterium".[39–45] The basis of research is the chemical shift of protons in the nuclear magnetic resonance spectrum. The greatest influence on such chemical shifts has local diamagnetic currents, paramagnetic currents acting on further distances and annular electron currents. In case of fullerenes, aromaticity as assessed by magnetic criteria reflects reactivity and stability.

The "geometrical criterion" says that in aromatic compounds, the carbon–carbon bond lengths are the same, and single and double bonds cannot be distinguished.[34,35,46–52]

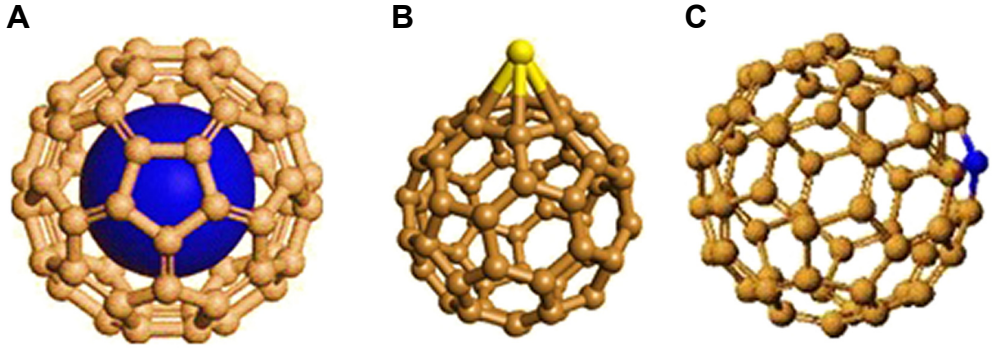

Figure 7 Endohedral fullerene (**A**), exohedral fullerene (**B**) and heterofullerene (**C**).

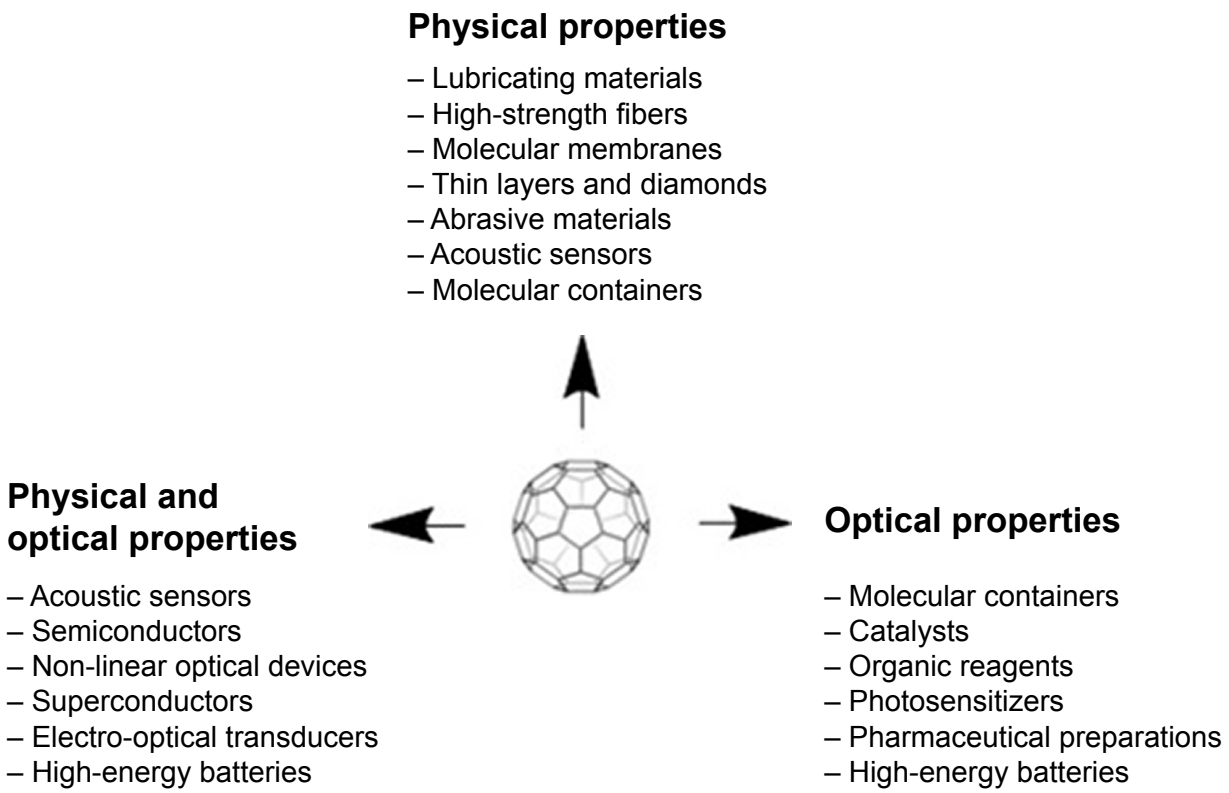

Figure 8 The physicochemical properties of fullerenes.
Note: Data from Kadish and Ruoff.[53]

The most frequently used index of aromaticity based on this criterion is the Harmonic Oscillator Model of Aromaticity (HOMA) index. Originally defined for hydrocarbons, it was later extended to heteroatom-containing compounds. The "structural/geometric criterion" predicts for C_{60} bond length variation between [6,6]- and [5,6]-bonds. Based on experimental data, the [6,6]-bonds are shorter than [5,6]-bonds in neutral fullerenes.

As the carbon allotropy has a dominant role in the nano-field, both for theoretical reasons and for further application prospects, the following carbon structures were tested: fullerenes, nano-pipes, graphite, diamond and spongy blocks of CNTs, namely, from zero-, to three-dimensional structures. In this way, several articles and several chapters of books were created.

Circulenes

A circulene is a molecule that looks like a flower[17] with a core and surrounding petals. The general formula is $[n:(p_1,p_2)_{n/2}]$, where n is the size of the core polygon and p_i are the polygonal petals. For n>6, the molecule is saddle shaped, whereas for n<6, it has a bowl-shaped geometry.[54–56] The second type of circulenes is useful in the synthesis of fullerenes,[57,58] while the first type can be found in the spongy carbon.[59–61]

Two types of fullerenes, one with joined patches and the other one with disjoined patches, are shown in Figure 9.

In Figure 10 are shown coronene $[6:6_6]$, isocoronene $[6:(5,7)_3]$ and sumanene $[6:(5,6)_3]$[63] circulenes.

The stability of the considered polycyclic compounds was estimated on the total energy per C atom and highest occupied molecular orbital(HOMO)-lowest occupied molecular orbital (LUMO) gap,[63] which can represent chemical hardness and is also an indicator of the molecular kinetic stability. The aromatic character of various flowers was estimated on three criteria: magnetic nuclear-independent chemical shifts (NICS)[62] (1 Å above and below the geometric center of gravity of the ring and in the middle of the aromatic ring), energetic (heats of formation) and geometric HOMA index (Figures 9 and 10).[63]

Diamond D5

Diamond D5[8,16,64] is a hyperdiamond with pentagonal rings, built up on the frame of mtn structure, appearing in clathrate hydrates of type II. The C_{17} (centrohexaquinane)

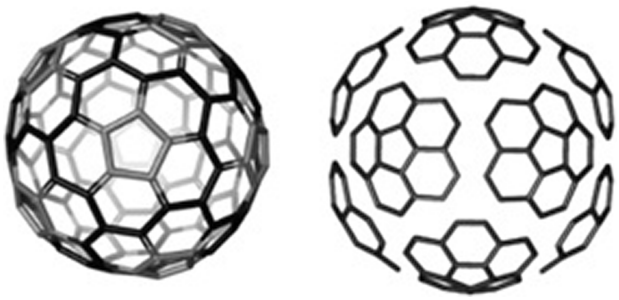

Figure 9 The [5:6^5] patch in fullerenes: joint patch in C_{140} (left) and disjoint patch in C_{240} (right).

was proposed[64] as the seed of D5. However, the classical diamond is Diamond D6[66–72] (Figure 11A), built of hexagonal rings with sp3 carbon atoms, and it is used in technology and jewelry because of its mechanical characteristics and esthetic appeal. Ultrasound cavitation,[73] chemical vapor deposition and high pressure–high temperature are applied to produce synthetic diamonds. A hexagonal network is called lonsdaleite (space group P63/mmc),[74] and several diamond-like networks have also been proposed.[65,75,76] Some multitori were proposed by Diudea and Ilíc[77] (Figure 11C). For example, the name of diamond D5 was given by Diudea[8,16,64,77,78] for structures with pentagonal rings.[8,16,64,77] As it was presented earlier, the seed of this diamond is C_{17} centrohexaquinane earlier studied by Gund and Gund,[79] Paquette and Vazeux[80] and more recently by Kuck.[81–83] The hyperdiamond D5 belongs to the space group Fd-3m[84,85] and is built up in the frame of mtn structure as a trinodal net. However, D5 belongs to the type II clathrate C_{34}.[86] This family of clathrates is a Si_{34}-analog, which was already synthesized. C_{34} is the repeating unit of the diamond D5 network and is formed by dimerization of two molecules of C_{17} (Figure 11B). An adamantine ada_20_158 (Figure 11D, left) can also condense to form the diamond D5 network (Figure 11D, right). The main unit of the hyper-diamond D5 can be C_{20}. In a large enough network, the ratio C-sp3/C-total renders to 1. The net is called the diamond D5[8,16,64] because most of the rings in the molecule are pentagonal.

During the study of diamond D5, four carbon structures were investigated based on C_{17} skeleton, built of carbon atoms or from carbon and oxygen atoms. The research was carried out using the molecular dynamics (Amber) and the ab initio methods at discrete Fourier transform (DFT) level. The structural stability was assessed on the basis of root-mean-square deviation (RMSD) and the total potential and kinetic energy obtained after molecular dynamics simulations. The four hypothetical seeds of D5 were used for structural and energy stability studies of the all-carbon structure C_{17} and the ones built from carbon and oxygen atoms (trioxa derivatives of C_{17}), as shown in Figure 11. The isomer P1 was synthesized by Paquette and Vazeux[80] (Figure 11C), while D_1 and D_2 were proposed by Diudea[8] (Figure 11E). The last structures would be used in dimerization to C_{34}, with the repeating unit[86] called D5.

The all-carbon seed C_{17} was the most resistant to changes in temperature during all molecular dynamics, while D_2 isomer was the most sensitive to changes in temperature among the four studied structures. The structural stabilities of P_1 and D_1 isomers were similar and only slightly more sensitive to temperature as compared with the all-carbon C_{17} in molecular dynamic (MD). The structure of D_1 was the most stable also after optimization at the DFT level of theory.

In the future, the results can have a practical aspect and can be used for dimerization reactions to C_{34} and condensation to adamantane-like structures, finally leading to diamond D5.

Polybenzenes

The structural stability (Hartree–Fock [HF] level, DFT) with respect to C_{60} as well as to diamonds (D5 and D6) has also been estimated for polybenzenes.[15] O'Keeffe et al[87]

Figure 10 Circulenes with hexagonal core: coronene (left); isocoronene (middle) and sumanene (right).

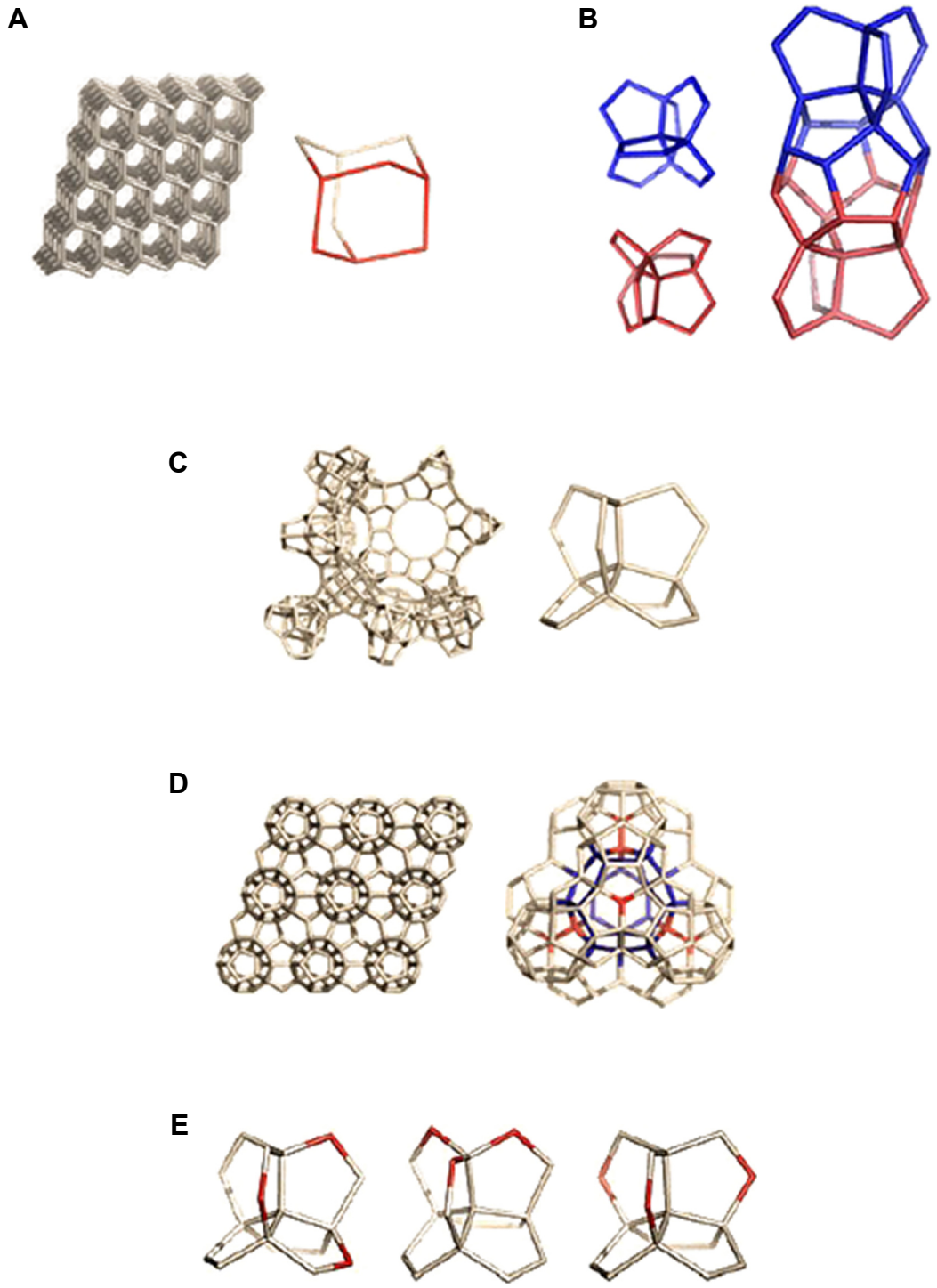

Figure 11 The repeating units, in crystallographic terms, of the diamond D5 and D6 networks.
Notes: (**A**) Diamond D_6 and its repeating unit adamantane. (**B**) Two C_{17} units give a dimer C_{34}; (**C**) the C_{17}; (**D**) adamantane; (**E**) C_{17}_hexaquinane triooxo-derivatives: Paquette P_1 and Diudea, D_1 and D_2.

projected two kind of structures: 6.8^2 *D* (polybenzene, Figure 12), belonging to the *Pn*3*m* space group with the topology of diamond, and 6.8^2P, belonging to the *Im*3*m* space group, similar to *P*-type surface. Both described structures show higher stability compared to C_{60}. The 6.8^{88} *D* that can stay as an insulator, 6.8^{88} *P* that is metallic, as well as zeolites and spongy carbon represent schwarzite structures.[88–91]

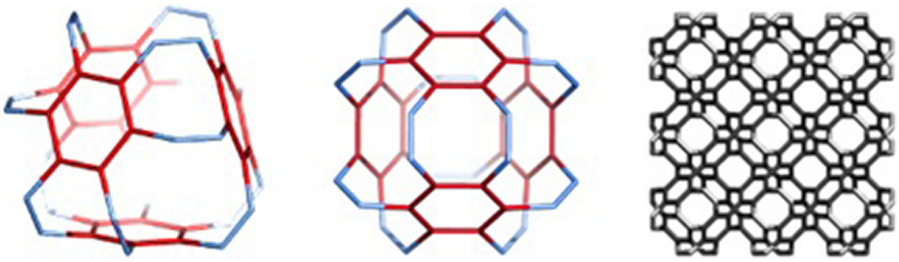

Figure 12 Benzene rings in the D-surface; BTA_48=6.82 D (left) BTA_48 unit (middle) and its diamondoid BTA_f_{cc}-network (in a [K,K,K]-domain, k=3, right).

Polybenzenes can spherically evolve or show linear periodicity (Figures 12 and 13). In this way, two structures are created, namely, BTA_48 and BCZ_48, respectively (Figures 12 and 13, left), colloquially called an armchair (BTA_48) and a saddle (BCZ_48). Tetrahedral unit BTA_48 can be possibly identified either by octagons R(8) or by dodecagons R(12). Identification by R(8) leads to 6.8^2 f_{cc}-net (Figure 12, right), with the topology of D_6-diamond.[92,93]

There are oligomers of BTA_48 such as BTA_{2ecl}_90 (Figure 14, left) and BTA_{Cy5}_210 (Figure 14, middle) and the multitorus BTA_{20}_780 (Figure 14, right), where the second structure can be built of the first and the third structure can be built of the second by self-arranges, respectively.

The 3-periodic net $BTZ24_{anti}$_333 with $\{6.9^2\}$; 3-c net "*uta*" belongs to the *Fd*-3*m* space group (Figure 15). A quasi-spherical structure of icosahedral symmetry can be created by 12 units of BTZ_{20} in self-arrangement. The 1-periodic networks can be formed by the units BTA_{20} and BTZ_{20} (Figure 15).

The results showed a significant stability of these structures, which gave a further perspective on their synthesis in the laboratory. Therefore, the Raman spectra and the infrared spectra were tested.

After calculations, the most stable were BTA_48 and BCA_96, both structures with values of Etot/atom(au) equal to 38.156 au. On the other hand, the least stable structure was BCZ_72 (Etot/atom(au) equal to 38. 056 au). However, the BCZ_48 structure showed the highest value of geometry index of aromaticity HOMA (0.989).

As suggested O'Keeffe et al,[87] the stability of polybenzene based on HOMO–LUMO HL gap and values of Etot/C was over that of the reference C_{60} fullerene and resembled the stability of diamond networks.

The values of Etot/atom, HOMA and HOMO–LUMO gap calculated after optimizations at HF (HF/6–31G**) and DFT (B3LYP/6–311+ G**) levels of theory revealed that the stability of dendrimers decreased monotonically with the increasing number of atoms, and also, the dendritic dimer was less stable than the dia-dimer. Compared to the reference C_{60}, all tested polybenzenes, that is, dendritic dimer and dia-dimer were very stable.

During the study, a structure construction of the network units of polybenzene, described by O'Keeffe et al,[87] was proposed. Their stability, relative to fullerene C_{60} and diamonds D5 and D6 was estimated at the HF level of theory. The calculations carried out confirmed their stability. The practical aspect of computational work is clearly visible here, which is obviously worth emphasizing.

Polybenzenes multitori

Multitori[9,10,14] are complex structures consisting of more than one single torus.[94–97] They include negatively curved

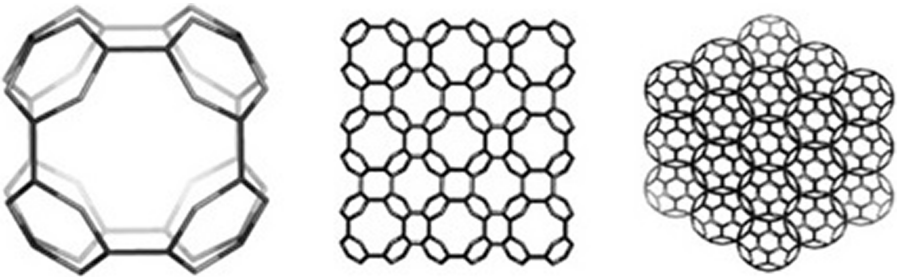

Figure 13 Benzene rings in the *P*-surface; BCZ_48=6.8^2 *P* (left), its networks in a cubic (*K*,*K*,*K*)-domain, *k*=3 (middle) and the corner view of this network (right).

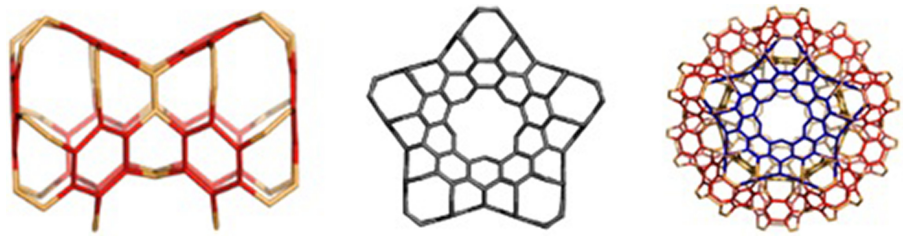

Figure 14 Oligomers of BTA_48: BTA_{2ecl}_90 (left) and BTA_{Cy5}_210 (middle) and the multitorus BTA_{20}_780 (right).

substructures,[98–100] termed schwarzites.[98–102] Multitori appear in natural zeolites and in spongy carbon, formed by self-assembly of repeating units. Multitori can show a linear periodicity or they can develop spherically, creating systems of different complexity.[103] The map operations[103–109] were used for design of Multitori with CVNET[110] software and Nano Studio.[111] Multitori, similar to rods, show a linear periodicity or can spherically evolve, and in this way were formed the polybenzenes multitori BTZ and BTA. The multitori BTA ("armchair") were compared to the ("zig-zag") BTZ (Figure 16).

The calculations at the HF level of theory (HF/6–31G**) were performed in the gas phase using Gaussian 09[112] program, and based on HOMO–LUMO gap and the total energy/carbon atom, the energy and structural stability were estimated. Also, using JSChem program,[113] the strain energy values were estimated. As usual, the C_{60} structure was taken as the reference. The analysis of the obtained results showed that BTZ multitori were as stable as C_{60} fullerene. Even so, BTA are more energetically stable compared with BTZ, which makes them more likely to exist in spongy coal or zeolite structures. BTZ multitori can be eventually synthesized in the laboratory.

Nanotube junctions

As described above, modeling of fullerenes and nanotube junctions[11,12] can be combined by using some mapping operations. In this way, high-generation dendrimers can be constructed. Again, the hypothetical nanotube junctions were constructed using CVNET[110] and Nano Studio[111] software programs (TOPO GROUP CLUJ-international scientific group created by prof. M.V. Diudea focus researchers from many countries, Babes-Bolyai University, Faculty of Chemistry and Chemical Engineering, Cluj-Napoca, Romania). Eight tetrapodal units were designed, where the energies were estimated at the HF level. Their stabilities are discussed in the scope of HOMO–LUMO space, energy of bonds and the HOMO aromaticity index and total energy.[34,35,46–52] The calculations were carried out by using G09[112] at the HF (HF/6–31G**) level of theory in gas phase. The open-end hydrogenated structures were used for calculations. As a reference structure, C_{60} was considered. During the synthesis of nanotube fullerenes, single- and multiwalled nanotubes, onion-fullerenes and others can appear. Experimentally, fullerenes can be spanned. In this way are built open cages. The open faces can be prolonged by nanotubes of various chirality and tessellation (most probably, a hexagonal one). Such spanned fullerenes (prolonged or not) are called nanotube junctions. They can be tetra-, octa- and icosahedral, when symmetry is taken into account.

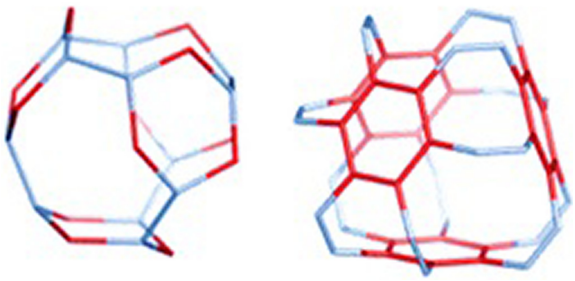

Figure 15 BTZ_24 (left) and BTA_48 (right) polybenzenes, open fullerenes.

The junctions (tetrapodal and tetrahedral) are very interesting. They exhibit similarity with the sp3 hybridized tetrahedral carbon atom. The valences are now nanotubes, while the atom is an opened cage embedded on the surface of genus 2.[114,115] As there is a single C atom, a tetrapodal junction can be used to build various nanostructures such as dendrimers and multitori multi torus (MT).

The connections the points of connectivity two of five units named TriPen_T_60A 60A and the dendrimer (at the first generation) with the patch of this unit called "tripentylene", $[6:(0,5)^3]$ (Figure 17). The unit TriPhen_T_60A can self-arrange, using map operations Le(Op(Ca(T))), to a pentagonal multitorus MT comprising five such units (Figure 18).

Next, using the map operations, from 12 pentagonal MT, the MT20[116–118] (a supra-structure) can be created (Figure 19).

After optimization of the study structures, *E*tot/C, HOMO–LUMO HL gap and the total energy of course were calculated (Table 1).

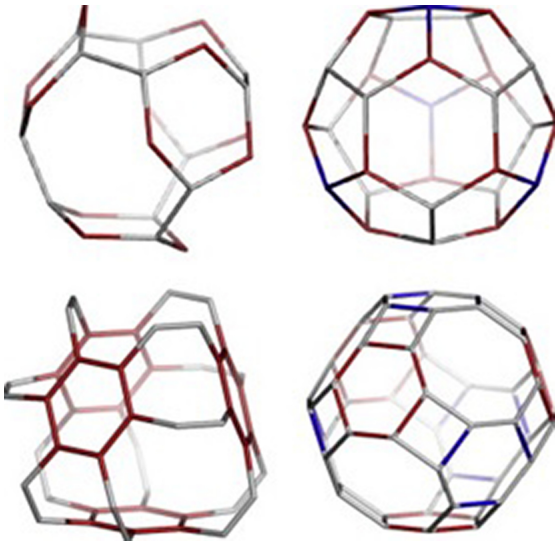

Figure 16 Top row: BTZ_24 designed from S2(T)_28=C28. Bottom row: BTA_48 formed by spanning the Le(P4(T))_48 cage.

The obtained values confirmed the possibility of using various nanotube junctions in further experimental work by welding the randomly superposed nanotubes. In comparison to C_{60}, the value of E_{HF}/C is favorable for tetrapodal junction. According to the Haddon's theory,[119–123] again, the HOMO–LUMO gaps are in favor of these open structures. Based on this part of the study, it can be concluded that the tetrapodal junctions can be used for the synthesis of new nanostructures in the laboratory.

In the next step, the CNT junctions can self-assemble into more complex structures, such as diamondoids and/or multitori of high genera.

The units were designed by using symmetry in embedding the triple hexagon patches (Figure 20, left column) or starting from the objects Op2a(S2(M)); M=Tetrahedron T or Cube C with deletion of one atom from each heptagonal face of the transformed map M (Figure 20, right column). An "eclipsed" dimer, the unit T_3HexZ_52 forms, which can self-arrange to a hyper-pentagon, and the joining of 12 such hyperfaces leads to a multitorus T_3HexZ20_1040 (Figure 21) of icosahedral symmetry.

An "intercalated" dimer is built from the unit T_3HextwZ_40, leading to a hyper-hexagon, forming diamondoids at the end (Figure 22).

The unit C_3HexZ_104 can build a multitorus as an infinite periodic lattice with k-the repeating unit embedded in the P-surface (Figure 23).

Examples are four units open to be inserted in exactly 4×2 simple tori and one more torus that joins all the above four units (Figure 24).

The Euler's theorem was applied to calculate the genus in a differently tessellated network (Figure 25).

The unit C_3HextwZ_80 can form a multitorus C_3HextwZ15_1200 (Figure 26). The six units of octahedron are joined by a central unit according to Cartesian coordinate directions. The eight units of the cube are connected to the centers of their faces by the diagonal directions (Figure 26, middle). In this way, as in the diamond, the octahedron fits the face-centered cube positions. Thus, the cube accommodates the vertices of its dual (the octahedron) in the center of its faces and one unit in the cube/octahedron center. Among any four units there is a hollow space; the structure can evolve periodically in a single direction (Figure 26, right).

It can be concluded that stability of the investigated junctions is comparable with the reference fullerene. The closest values to the reference structure show "twisted" junctions (Table 2). As expected for structures with larger "open" faces, the strain is lower for the octahedral junctions. Because the twisted structures are more anti-aromatic in comparison to the non-twisted ones, the geometric index of aromaticity HOMA is not relevant.[121]

The vibrational spectra of study junctions were simulated, which identified the differences between twisted and non-twisted structures and between the two different embeddings (tetrahedron and cube).

Based on this part of research, it can be concluded that various nanotube junctions could appear in real experiments by welding, under an electron beam, of the randomly superimposed nanotubes.

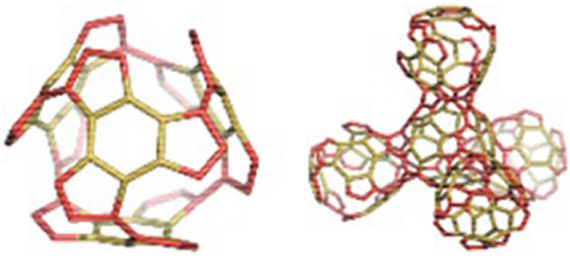

Figure 17 Dendrimer (right) and TriPen_T_60A (left).

Spongy nanostructures

Spongy structures[18,84] are high-genera and large nanostructures with characteristic holes on their surface. Some new structures, spongy polyhedral, were proposed for research. They can evolve with 1-periodicity or radially, to provide multi-shell cages.

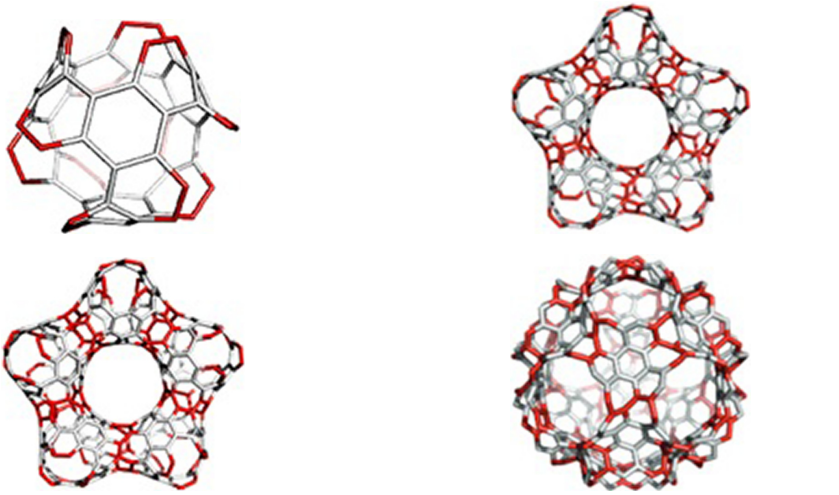

Figure 18 Top row: TriPhen_T_60A (left) and a pentagonal hyper-ring (right). Bottom row: Multi-torus MT(Le(Op(Ca(T)))); [Op($Ca_{(3,2)}$C(I))] (left) and its core (right).

Because of the large number of atoms, that is, >1,500, the density functional-based tight binding (DFTB) method[124,125] was used for computing of these structures. This method was combined with the self-consistent charge (SCC) technique and resulted in SCC–DFTB method.[126] In this way, the results obtained were comparable with some higher-level theoretical methods.[127–129] The SCC–DFTB geometry optimizations were performed using the DFTB+ program.[125] DFTB is useful in the case of large nanoparticles. For this reason, it has certain drawbacks, such as underestimation of the gap values in the case of sp2 carbon-only structures and overestimation of the gap values for the hydrogenated ones. Gaussian 09[112] was used in the case of some structures with level of calculations HF and DFT and 6–31 g (d,p) basis set. The small radius of C_{20} (ie, large pyramidalization angle of sp2-hybridized carbon atoms) causes an extremely high reactivity/instability of the dodecahedron-based structures, such as carbon-only structures, but they become more stable by hydrogenation.[124] For reference, the fully hydrogenated $C_{60}H_{60}$ was chosen here. One can see that full hydrogenation of the dodecahedron as $C_{20}H_{20}$causes structural stabilization (Table 3). The values for the included structures show, however, a lower stability; the spongy cage Do(Do20)_250H100 (Table 3) is more stable than the corresponding filled structure Do@ Do(Do20)_270H80. Passivation by full hydrogenation, resulting in a far deeper gap, is important in the case of structures presented in Table 4. One can see that the filled structures (Table 4) have values of HOMO–LUMO gap lower than the spongy ones, meaning a larger kinetic instability. Looking at the C_{60} dimers analogous to the hyperdimers on 750 and 810 atoms (figure in Table 5 and entries 5 and 6), the same ordering can be found in Table 4 for the carbon-only dimers: Gap ($C_{60}P_2J_5$_115) > Gap($C_{60}P_2J_6$_114); this could be a result of the fact that joining by pentagonal faces (J5) results in more hexagonal faces, involved in double-bond conjugations, thus stabilizing the whole structure. Conversely, the passivation by hydrogenation is more effective in the case of J6-dimer, which is more reactive than the carbon-only molecule. Three series of calculations were made on DFTB, HF and DFT levels of theory to see if the ordering of stability is influenced or not by the used approach. We can see that because the calculations are made in vacuum (no solvation process involved), the ordering is preserved in these three approaches.

Compared to fullerene C_{60}, the structures built up by C_{60}&C_{24}&C_{10} show the highest stability (Table 5). The values of HOMO–LUMO gap and energy/atoms (in DFTB) in the case of cages with 300 and 900 atoms are higher than in case of C_{60}. These multi-cages contain the C_{60} fullerene non-coalesced with itself but separated by smaller cages C_{24} and C_{10}. The last structure in Table 6 also represents an aggregation of C_{60}, with the units sharing a pentagon, while the interspaces have the topology of twin-truncated tetrahedral TT. It is relatively less stable as carbon-only structure, compared with the non-coalesced C_{60} structures. Hydrogenation of rod-like structures based on C_{60} & C_{12} aggregation (Figure 7) could provide stable, useful materials (Table 7).

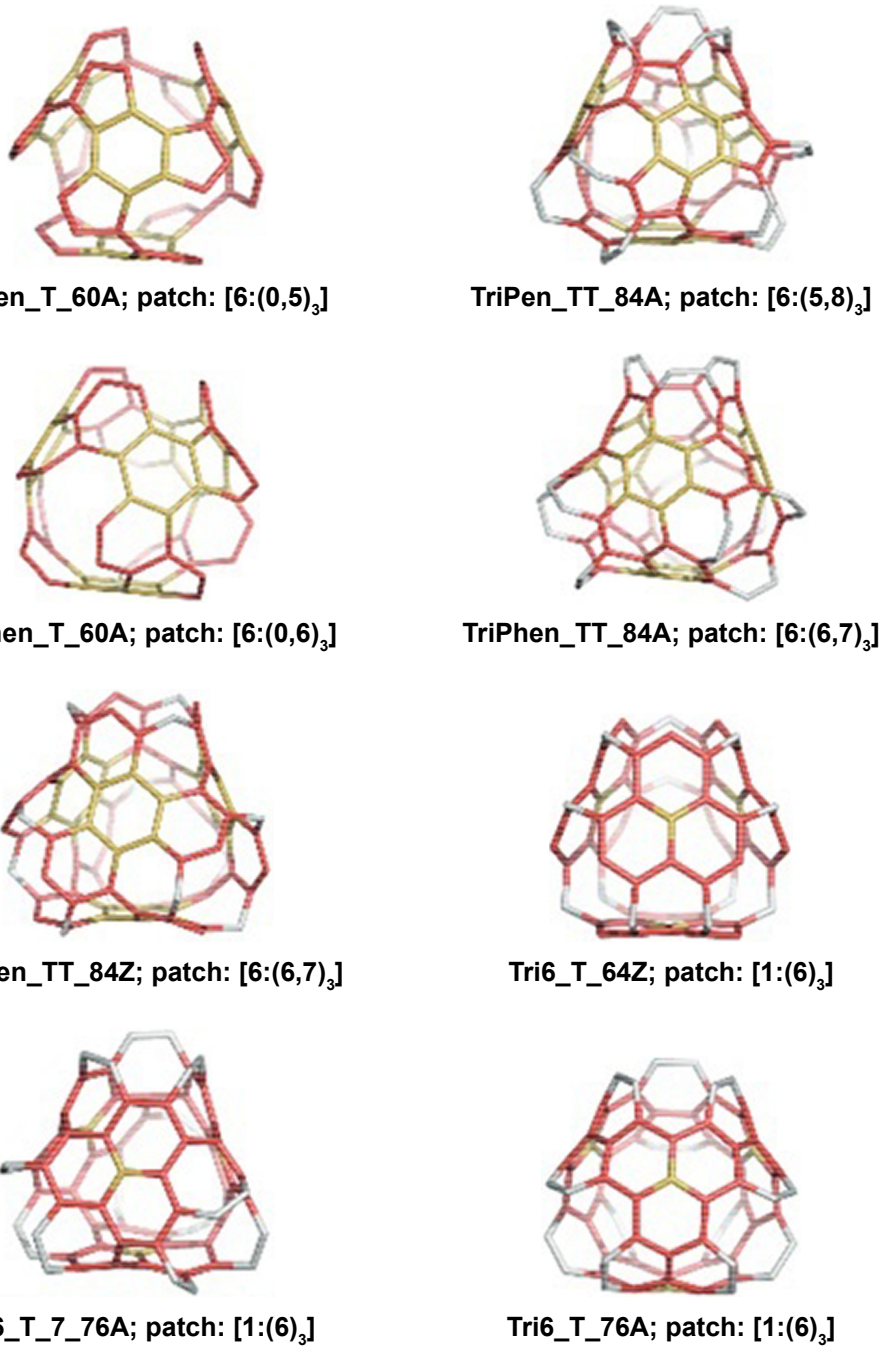

Figure 19 Tripentylene, triphenylene and hexagon triples as tetrapodal nanotube junctions.

Fullerenes in medicine: how nanotechnology extends diagnostic and therapeutic possibilities?

There is a reasonable belief that the most important future applications of fullerenes lie in the field of medicine. After all, carbon is the basis of all living organisms and the fullerene discovery can certainly be compared to the discovery of benzene, whose derivatives account for 40% of all drugs, even the most popular aspirin. The C_{60} molecule can bind to any functional group. At the same time, it is indifferent, nontoxic and so small that it easily comes into contact with cells, proteins and viruses. In addition, its interior can also be filled with active substances. During working on small objects, we observe a very important feature, mainly increasing the surface to volume ratio, which makes the molecules chemically more reactive. Only this single feature makes it

Table 1 Tetrapodal nanotube junctions and their energy properties[a]

	Structure	E_{HF}/C (au)	HL gap (eV)	Strain/C $\times 10^3$ (kcal/mol)	HOMA patch	Kekulé count
1	TriPen_T_60A	–38.092	7.191	21.873	–0.455	128
2	TriPen_TT_84A	–38.028	7.043	12.004	–0.401	12500
3	TriPen_T_60A	–38.095	8.070	21.120	0.222	1944
4	TriPen_TT_84A	–38.029	7.762	11.696	0.283	12500
5	TriPen_TT_84Z	–38.023	4.815	42.630	0.493	256
6	Tri6_T_64Z	–38.082	5.824	37.971	0.636	0
7	Tri6_T_7_76A	–38.046	6.250	11.276	0.279	2700
8	Tri6_T_76A	–38.047	5.612	19.566	0.340	9504
9	C_{60}	–38.864	7.418	137.600	0.493	12500
10	Triphenylene	–38.260	10.378	0	0.678	9

Note: [a]C_{60} was used as a reference structure.
Abbreviation: HOMA, Harmonic oscillator model of aromaticity.

possible to drastically reduce the dose of the drug without impairing its therapeutic effect. Nanotechnology has allowed the development of new materials (called nanomaterials) with a number of properties that are desirable, such as antibacterial effect, magnetic excitation, increased conductivity or electrical resistance, increased resistance to corrosion and abrasion and increase in plasticity. That is why, they can be used in medicine.

The main problems regarding the use of fullerenes in medical chemistry were their insolubility in polar solvents, as well as formation of aggregates in aqueous solvents. However, these problems have been solved through a series of chemical modifications of fullerene molecules. Therefore, the so-called exo- and endohedral functionalization is carried out (Figure 27).

The essence of exohedral chemistry is the chemical reactions of attachment occurring "outside" the fullerene molecules, in which the structure of the carbon cage remains unchanged (Figure 27). The prospects of fullerenes' connections are huge, as there are an astronomical number of isomers. In "Chemical Abstracts" – the basic source of citations of chemical literature in this field in the world – there are already >5,000 known fullerene derivatives. Unlike other organic, aliphatic and aromatic compounds, fullerenes do not contain hydrogen atoms or other functional groups, so they cannot undergo substitution reactions (except heterofullerens). Substitution reactions occur only with "functionalized" fullerenes, that is, when they have been attached to specific groups of atoms.

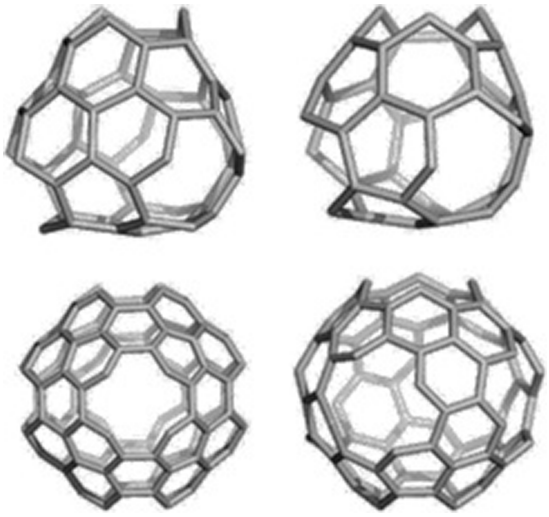

Figure 20 T_3HexZ_52 (top, left), T_3HextwZ_40 (top, right), C_3HexZ_104 (bottom, left) and C_3HextwZ_80 (bottom, right).

Exohedral fullerenes

The exohedral reactions of fullerenes are mainly based on the attachment of radicals or functional groups to carbon atoms by saturating the double bond. Exohedral chemistry of fullerenes is extremely rich and covers all basic areas of organic functionalization (Figure 27). The research concerns mainly C_{60} and, to a lesser extent, C_{70}. Fullerenes, C_{60} and C_{70}, can take part in many different reactions, including the most typical – reduction and oxidation. Reduction – joining reactive atoms, most often hydrogen atoms, to the outside of the carbon cage – is carried out by various techniques, and currently, the most hydrogenated fullerene is $C_{60}H_{36}$. Also, fullerenes can be oxidized, with the C_{60} molecule being less resistant to pure oxygen than graphite at a temperature of about 500 K. Mild oxidation leads to the formation of epoxide compounds of the $C_{60}O_n$ type, where n may vary from 1 to 4 and carbonyl groups appear in the molecule without disturbing the structure of the molecule. An interesting group of derivatives are fulleroles, substituted with hydroxyl groups, which are soluble in water. $C_{60}X_n$ halogen derivatives have also been synthesized, where X is fluorine,

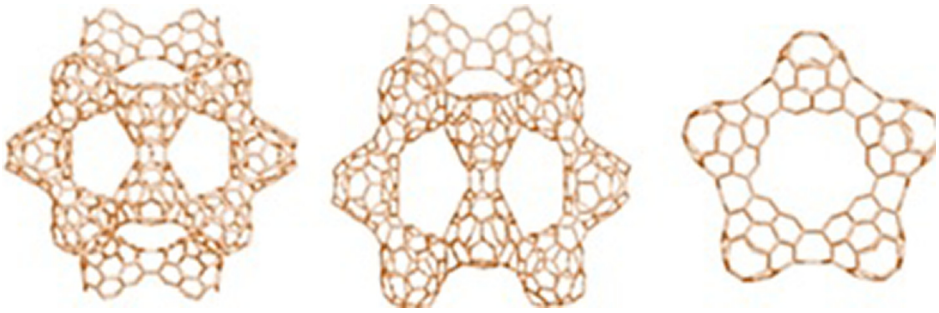

Figure 21 Multitorus T_3HexZ20_1040; g=21 (left) built up by T_3HexZ_52 and its substructures: T_3HexZ10_520; g=11 (middle) and a hyper-pentagon T_3Hex5_260; g=6 (right).

bromine or chlorine and n can reach 60. Metallofullerenes are complex compounds of fullerenes with metals, in which the metals are elements from the platinum group and they have interesting catalytic properties (Figure 27).

Endohedral fullerenes

From the beginning, the fullerene explorers had the idea that an empty "cage" of fullerene could be filled with something (Figure 27). The diameter of C_{60} is 0.7 nm, so the interior of the molecule can be a "container" for other atoms of any size or can be a reactionary environment of endohedral chemistry, "intraframe" chemistry. The internal atom is insulated from the environment and, at the same time, the exchange of electrical charge. This results in interesting properties, for example, pure C_{60} is an electrical insulator and after taking over the metal charge, it can become a conductor. The fullerenes having an alkali metal atom its inside show superconductors properties and they are not sensitive to contact with air.

Heterofullerenes

Heterofullerenes are fullerenes in which a partial substitution of the carbon atom (s) in the C_{60} cage structure takes place by atoms of other elements, most commonly boron and nitrogen atoms. However, it has not been possible to obtain macroscopic quantities of such heterofullerenes to enable detailed examination and verification of their interesting properties (Figure 27).

Cyclodextrin

The main problems concerning the use of fullerenes in medical chemistry are their formation of aggregates and insolubility and the formation of aggregates in aqueous solvents (polar solvents). However, these problems have been solved by a series of chemical modifications of fullerene molecules. Fullerenes can be closed in cyclodextrins, which mask the carbon sphere, thereby increasing the solubility of such derivatives in polar solvents. Due to the size of C_{60}, the most common β-cyclodextrin cannot be used directly (Figure 28). Hence, for the carbon masking of the sphere, dextrins of larger sizes are used, which form C_{60} complexes in a 2:1 ratio.[130] To create the possibility of using s-cyclodextrin to form a complex with the C_{60} molecule, fullerene was converted to a biphenyl derivative (Figure 28).[131]

Fullerene derivatives were also obtained by adding different hydrophilic groups to C_{60}. The more such groups the fullerene molecule has, the greater its hydrophilicity. An example of such derivatives is the fullerene dendrimeric derivatives. The dendrimeric C_{60} derivative, having specifically carboxylic groups (Figure 29), shows a high degree of solubility in water.[132] Cycloaddition processes are a large group of fullerene functionalizations (fullerene cycloadducts),

Figure 22 Diamondoids built up by T_3HextwZ_40: Ada_400; g=11 (left), Dia_560; g=15 (middle) and the network T_3HextwZ_(2,2,2)_1760; g=45 (right).

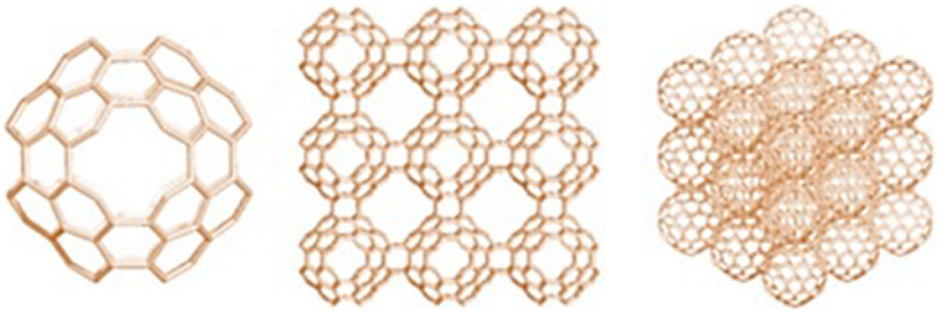

Figure 23 C_3HexZ_104, *g*=3 (left), its P-type-crystal network C_3HexZ_(3,3,3)_2808 (middle) and the same array in the corner view (right).

which create the possibility of synthesis of a wide range of new compounds, for example, the preparation of macromolecular fullereno-dendrite is based on the addition of phenolic groups in the first stage, to which the dendritic macromolecule is then attached.

All modifications of fullerenes, by the attachment of different functional groups or entire molecules of chemical compounds, cause an increase in the hydrophilicity of derivatives and also contribute to the preparation of new compounds which exhibit biological and pharmacological activity. The properties of the new derivatives are slightly altered, but they still exhibit the characteristic physical and chemical properties of fullerenes.

Fullerenes can act as antioxidants, protect nerve cells, prevent cell apoptosis, act as enzyme inhibitors, have antibacterial and antiviral effects, and it is also planned to use fullerenes for the treatment of osteoporosis. Above all, they have already found quite a significant place in cancer diagnostics since nanostructures represent the future in anticancer treatment, and have also found application in cosmetology.

Dendrimers and fullerene derivatives

In the course of neurodegenerative diseases such as Lou Gehrig's, Parkinson's or Alzheimer's, overproduction of ROS occurs. ROS are natural products of metabolism, but sometimes their concentration may increase rapidly leading to a phenomenon called oxidative stress. Too much ROS cause damage or death of the neuronal cell due to their oxidizing action. In such cases, it is beneficial to introduce a radical-scavenging agent that, although does not eliminate, significantly decreases neuronal mortality. Such antioxidant factors may be fullerene hydroxyl derivatives, fullerenols, which are excellent and are able to neutralize oxygen radicals. Fullerenols also reduce the toxicity of free radicals in the nervous tissue.[133] In contrast, other fullerene derivatives, carboxylefullerenes (Figure 30), show effective counteracting action against the degradation of neuronal cells associated with amyotrophic lateral sclerosis.[134] Fullerenes can also prevent self-destruction, namely, apoptosis. It is a biochemical process of cells in which transforming growth factor-β plays an important role. During this process, ROS induction occurs and the only way to stop or at least reduce the scale of cell destruction is the use of antioxidants. Such properties are shown by fullerene carboxyl derivatives. Nanostructures may prevent apoptosis in some cells by neutralizing the ROS induced by transforming growth factor-β.[135]

Figure 24 Multitorus C_3HexZ4_1184; e=1776; f6=496; f7=64; f8=16; *f*=576; by Euler formula, *g*=_(1184_1776+576)_2)/2=9; by theorem 2, *g*=2_4+1 (in black/red)=9.

Numerous studies have been carried out on the nucleotide chain cleavage process in the presence of fullerene derivatives. This phenomenon occurs only in the presence of light and has been tested in bacterial cells and plasmids.[136] It is believed that one of the steps of the oligonucleotide chain cleavage mechanism is the photon excitation of fullerene, followed by the transformation of molecular oxygen into the induced singlet state $^1O_2$. Then, fullerene returns to the basal state and, at the same time, the interaction of reactive $^1O_2$ with the oligonucleotide occurs.[137] The proposed mechanism is shown in Figure 31. This process can also be used in photochemotherapy[137] and, in particular, in the treatment of skin cancer.

Some fullerene derivatives (Figure 32) may be inhibitors of enzymes such as serine proteases and cysteine

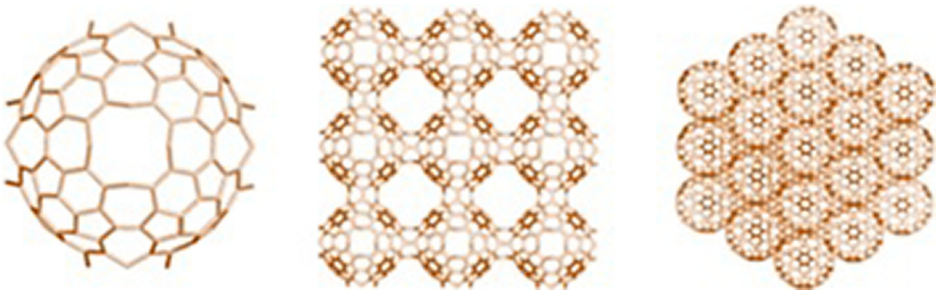

Figure 25 Sum_CZ_192, g=3 (left), its P-type network Sum_CZ_(3,3,3)_5184 (middle) and its corner view (right).

proteases.[136] Fullerenes of *S*-glutathione transferase,[138] cytochrome P450 monooxygenase and mitochondrial ATPase were also found.[139] Electrophilicity and hydrophobicity with high reduction potential are the key elements of fullerenes' activity toward enzymes. It is also expected that among fullerenes, effective anti-AIDS drugs will be found. The C_{60} derivative, which is an HIV protease inhibitor, has already been synthesized (Figure 32). The molecule fits the active viral protease center and strongly interacts with the van der Waals forces.[140] Modifications of fullerene derivatives are still underway, aimed at a stronger interaction with HIV protease inhibitor and the most effective blocking of the enzyme.

The lipophilicity of the carbon sphere allows the incorporation of C_{60} into biological membranes, causing them to destabilize, which enables them to be used as antimicrobial agents[141] against *Bacillus subtilis*, *Mycobacterium avium*, *Candida albicans* and *Escherichia coli*.[142,143] The fullerene salts proved to be very effective. Attention should also be paid to fullerenopeptides.[144] The peptide derivative of fullerene (Figure 32) shows lipophilic properties with hydrophilicity and the ability to undergo electrostatic interactions, which is derived from the peptide part, makes them exhibit antibacterial properties. *E. coli* and *Staphylococcus aureus* bacteria were tested, which showed sensitivity to this derivative. An analogous peptide lacking the fullerene part (Figure 32) showed no activity against these bacteria.[145] In addition, fullerenopeptides may have different effects depending on the type of bacteria – acting more strongly on Gram-positive bacteria and less strongly on Gram-negative bacteria.[146]

It is also hoped that fullerenes can be used to treat osteoporosis. Currently, in the treatment of this disease, diphosphate compounds and the F^- anion are used. However, diphosphate drugs are not effectively absorbed from the gastrointestinal esophagus, and also, F^- administered in the form of NaF is highly toxic.[147–149] Diphosphate fullerene $C_{60}(OH)_{16}$AMBP (Figure 33) shows the ability to reduce hydroxyapatite mineralization.[150] Similar studies regarding compound $C_{60}(OH)$ indicated high affinity for hydroxyapatite. These results give hope for the use of these nanostructures in targeted therapy for this disease.

From a certain date, fullerenes have also been used as safe and effective contrast agents, iohexal and iopamidol. Only 2%–8% of the studied population exhibits allergic reaction after the contrast is administered. Therefore, it was looked for measures with longer duration of action, what could extend the observation time of the patient, and would be nontoxic for each patient. Because a fullerene cage is empty inside, it is possible to use fullerenes also in this field of medicine. A lot of isotopes have been placed in the middle of the carbon sphere, resulting in endohedral metallofullerenes.[151] Such molecules are characterized by high stability and lack of biotransformation, which prevents the release of toxic

Figure 26 C_3HextwZ15_1200, g=31, m=1 (left); its reduced graph, v=15, e=30 (middle) and a linear periodic array C_3HextwZ25_2000, g=52, m=2 (right).

Table 2 Structural and energetic properties for two types of triple hexagon patched nanotube junctions[a]

	Structure	E_{HF}/C (au)	HL gap (eV)	Strain/C (kcal/mol)	HOMA patch	Kekulé count
1	T_3HexZ_52	–37.986	6.140	5.435	–0.131	972
2	C_3HexZ_104	–37.999	5.342	2.329	0.258	944784
3	T_3HextwZ_40	–38.021	6.681	5.799	–0.583	72
4	C_3HextwZ_80	–38.036	6.050	2.551	–0.020	11025
5	C_{60}	–38.864	7.418	8.256	0.493	12500

Note: [a]As a reference structure, C_{60} fullerene was used.
Abbreviation: HOMA, Harmonic oscillator model of aromaticity.

isotopes during therapy. Attempts have been made to use endohedral metallofullerene 166Ho@$C_{82}(OH)_x$ as a contrast agent. This compound persisted in the blood over 1 hour, and after that it was almost completely removed from the body and showed no toxicity in vivo.[152,153]

There are also studies on the use of endohedral metallofullerene in MRI. Fullerenes can also be used as carriers of genes, proteins or medicinal substances.[154] It has been shown that the tetraaminofullerenic derivative can transport plasmid DNA.[155] Another fullerene derivative, $C_{60}(CO_2H)_2$, has the ability to penetrate cell membranes and connect specifically to cell organelles.[156] In the future, fullerenes may be used as drug carriers, in particular, highly polar molecules attached to the fullerene sphere, such as C_{60}-oligo DNA. Fullerene drug carriers can penetrate the cell membranes by transporting the drug to selected tissues.[157]

Extremely interesting chemical properties and specific construction of fullerenes give many prospective opportunities to use these carbon balls.

Nanoparticles used in medicine and pharmacy

Based on the field of usage of nanoparticles, they could be divided into silver, gold, copper, magnetic and core–shell nanoparticles, quantum dots, fullerenes and CNTs. However, in medicine and pharmacy, the magnetic nanoparticles (MNPs) such as fullerenes and CNTs are mostly used.

Magnetic nanoparticles

MNPs are built of an inorganic core, for example, cobalt, nickel or iron oxide, with a coating that is compatible with the tissues into which it is inserted.[158] Magnetic properties

Table 3 DFTB data for DO/C_{20}-based hydrogenated spongy structures (figure in the last row in the table); reference structure $C_{60}H_{60}$

	Structure	C atoms	Etot (au)	Etot/C (au)	Gap (eV)
1	$C_{60}H_{60}$	60	–125.584	–2.093	10.412
2	$C_{20}H_{20}$	20	–42.089	–2.104	10.880
3	Do@Do_{12}_130H_{60}	130	–247.251	–1.902	7.723
4	P_4TRS$(Do)_{12}$_110H_{80}	110	–219.994	–2.000	7.908
5	S_2(Do)_140H_{100}	140	–290.104	–2.072	8.290
6	Do(Do_{20})_250H_{100}	250	–465.370	–1.861	5.474
7	Do@Do(Do_{20})_270H_{80}	270	–491.660	–1.821	4.736

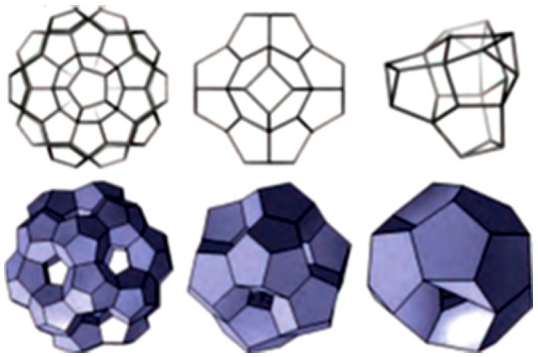

Spongy structures decorated by dodecahedron Do cages, derived from the platonic solids: dodecahedron (Do=C_{20}, left); cube (C=C8. middle) and tetrahedron (T=C4, right).

Table 4 DFTB data for the spongy C_{60}-based structures (figures in the last row in the table)

	Structure	C atoms	Etot (au)	Etot/C (au)	Gap (eV)
1	$P_4TRS(C_{60})\_330H_{240}$	330	−660.845	−2.003	8.816
2	$C_{60}@((C_{20})_{12}$ $(C_{24})_{20})\_390H180$;	390	−739.686	−1.897	2.507
3	$C_{60}(Do_{60})\_750H_{300}$	750	−1412.332	−1.883	7.937
4	$C_{60}@C_{60}(Do_{60})\_810H_{240}$	810	−1491.515	−1.841	2.660
5	$C_{60}(Do_{60})_2\_J5\_1410H530$	1,410	−2642.551	−1.874	7.831
6	$C_{60}(Do_{60})_2\_J6\_1392H516$	1,392	−2604.758	−1.871	6.552

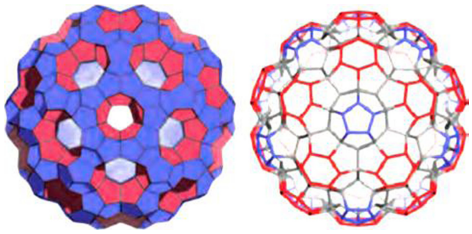

Spongy structure, Do decorated, derived from C_{60}: $C_{60}(Do_{60})\_750$ (also named RS(P4(C_{60}))330)@(S2(C_{60})420)_750, left) and its inside is hollow TRS($P_4(C_{60})$)_330 (right).

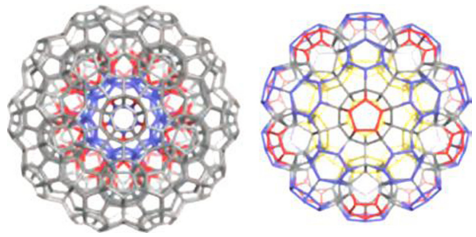

Filled form of the spongy structure $C_{60}(Do_{60})\_750$: $C_{60}@C_{60}(Do_{60})\_810$ (also named $C_{60}@((C_{20})_{12}$; $(C_{24})_{20}\_@Do_{60}\_810$, left) and $C_{60}(@(C_{20})_{12}$; $(C_{24})_{20}\_390$ (right).

Abbreviation: DFTB, density functional-based tight binding.

Table 5 Energy data for the C_{60} dimers (figure in the last row in the table)

	Structure	Theory	Etot (au)	Etot/C (au)	Gap (eV)
1	C_{60}	HF	−2,271.830	−37.864	7.418
	$C_{60}P215\_115$		−4,354.333	−37.864	7.597
	$C_{60}P216\_114$		−4,316.491	−37.864	6.270
2	C_{60}	B3lyp	−2286.174	−38.103	2.760
	$C_{60}P215\_115$		−4381.797	−38.103	2.907
	$C_{60}P216\_114$		−4343.730	−38.103	1.908
3	C_{60}	DFTB	−102.185	−1.703	1.930
	$C_{60}P215\_115$		−195.708	−1.702	2.044
	$C_{60}P216\_114$		−194.183	−1.703	1.444
4	$C_{60}H_{60}$	HF	−2306.420	−38.440	13.679
	$C_{60}P2J5\_115H110$		−4417.286	−38.411	12.252
	$C_{60}P2J6\_114H108$		−4378.295	−38.406	12.818
5	$C_{60}H_{60}$	B3lyp	−2321.937	−38.699	6.736
	$C_{60}P2J5\_115H110$		−4446.990	−38.669	5.708
	$C_{60}P2J6\_114H108$		−4407.716	−38.664	5.909
6	$C_{60}H_{60}$	DFTB	−124.582	−2.076	12.091
	$C_{60}P2J5\_115H110$		−236.608	−2.057	8.101
	$C_{60}P2J6\_114H108$		−234.229	−2.055	9.026

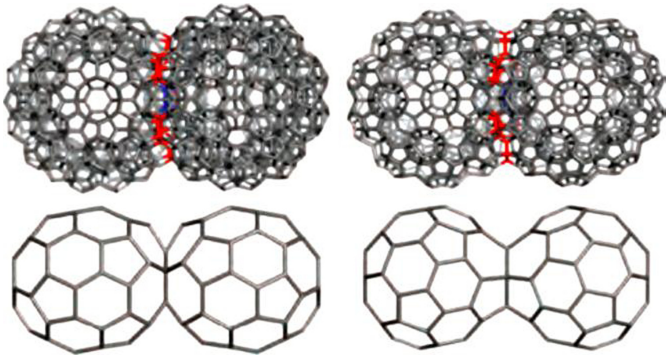

Rod-like dimers of $C_{60}(Do_{60})\_750$: C60(Do60_2_5_1410) (left) and $C_{60}(Do_{60}\_2\_6\_1392)$ (right) and the corresponding $C_{60}P2J5\_115$ and $C_{60}P2J6\_114$ simple C_{60} dimers (bottom).

Abbreviations: DFTB, density functional-based tight binding; HF, Hartree–Fock.

Table 6 DFTB data for spongy C_{60}-based structures, as carbon-only cages (figures in the last row in the table)

	Structure	C atoms	Etot (au)	Etot/C (au)	Gap (eV)
1	C_{60}	60	−103.292	−1.722	1.798
2	$C_{60}@((C_{10})_{12}(C_{24})_{20})$	300	−512.794	−1.709	2.845
3	$C_{60}@((C_{10})_{12}(C_{24})_{20})@((C_{10})_{30}; (C_{60})_{20})$	780	−1340.010	−1.718	1.024
4	$C_{60}@((C_{10})_{12}(C_{24})_{20})@((C_{10})_{30}; (C_{60})_{12})((C_{24})_{20})$	900	−1545.56	−1.717	2.452
5	$C_{60}@((C_{12})_{20}(C_{60})_{20})_{12})\_570)$	570	−980.894	−1.721	1.474

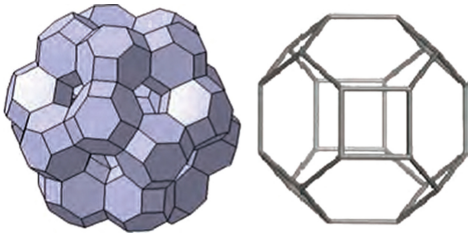

Spongy structure $C_{60}@(C_{24})_{20}$_300 (also named $C_{60}@((C_{10})_{12})$, $(C_{24})_{20}$_300, left) made from truncated octahedral TO (right); the window faces are just the pentagonal prisms P5=C10 (not seen).

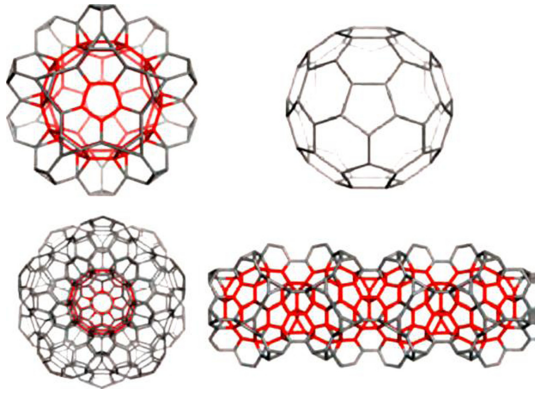

Radial and linear aggregation of C_{60} & TT/C_{12} small cages: $C_{60}@TT_{20}$_150 (or $C_{60}@(C_{12})_{20}$_150, left top), C_{60} (right top), $C_{60}@((C_{60})_{12}; (2\times TT)_{20})$_570 (or Le(Do@$Do_{12}$_130)_570, left bottom) and ($C_{60}@TT_{20}$_150)_4_465 (right bottom).

of nanoparticles depend on the presence and modification of surface ligands, size of the core and, first of all, on the composition. The MNPs show the property of superparamagnetism and are used in clinical diagnostic techniques. The introduction of MNPs into the examined tissue results in the disturbance of their local magnetic field, causing a reduction of relaxation time. This phenomenon is used in MRI.[159] The use of MNPs significantly improves the

Table 7 DFTB data for linearly aggregated C_{60} & C_{12} cages (figure in the last row in the table)

	Structure	C atoms	Etot (au)	Etot/C (au)	Gap (eV)
1	$C_{60}@((C_{12})_{20})\_1\_150H_{60}$	150	−279.799	−1.865	7.34
2	$C_{60}@((C_{12})_{20})\_2\_255H_{60}$	255	−471.215	−1.848	7.05
3	$C_{60}@((C_{12})_{20})\_3\_360H_{60}$	360	−662.630	−1.841	6.93
4	$C_{60}@((C_{12})_{20})\_4\_465H_{60}$	465	−854.045	−1.837	6.88

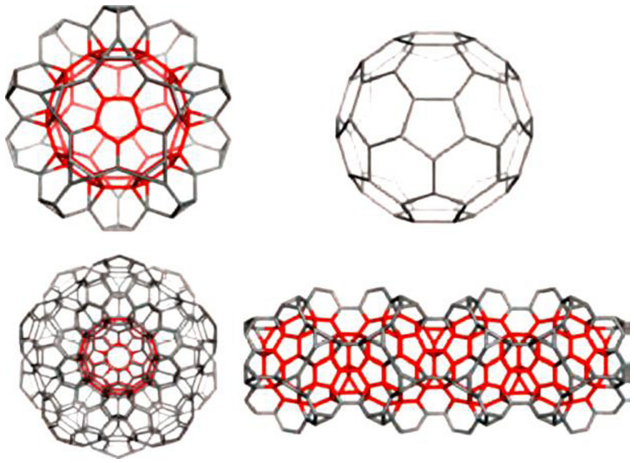

Radial and linear aggregation of C_{60}&TT/C_{12} small cages: $C_{60}@TT_{20}$_150 (or $C_{60}@(C_{12})_{20}$_150, left top), C_{60} (right top), $C_{60}@((C_{60})_{12};(2\times TT)_{20})$_570 (or Le(Do@$Do_{12}$_130)_570, left bottom) and ($C_{60}@TT_{20}$_150)_4_465 (right bottom).

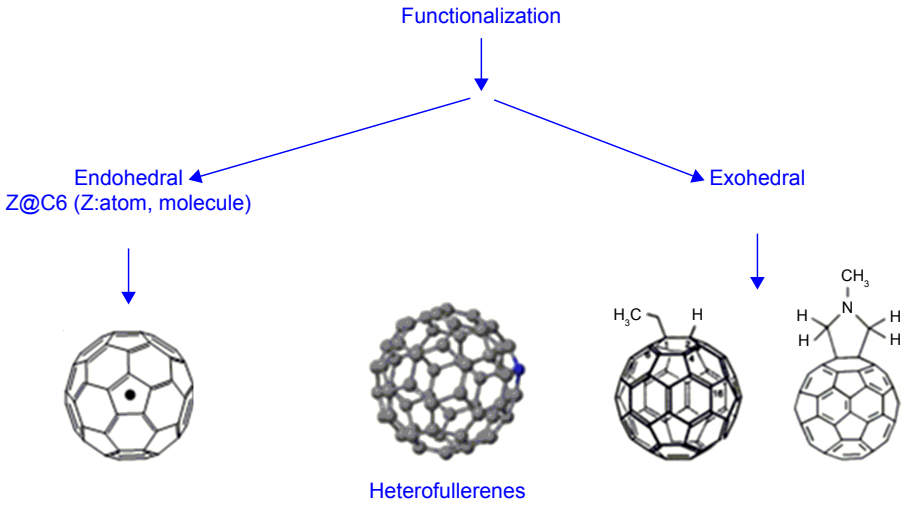

Figure 27 Exohedral, endohedral and heterofullerenes.

distinction between cancerous and healthy tissues. In addition to imaging tumor tissues, MNPs are used to observe the cardiovascular system, mainly in the detection of atherosclerotic plaques and other diseases of the cardiovascular system.[160,161] MNPs can be additionally combined with organic and fluorescent dyes, for example, rhodamine or fluorescein isothiocyanate, which allows to determine the extent of resection of tumor tissue in an intraoperative study. Another application of MNPs is the supply of pharmaceuticals to specific pathological tissues by using the affinity of the surface ligands used, magnetic attraction and by manipulating the external magnetic field.[159]

Biocompatibility, lack of toxicity and high accumulation in cancerous tumors enable magnetic nano-sized magnetic particles (NCz) also to be used in the so-called "intracellular" hyperthermia. This therapy involves the use of MNPs and a variable magnetic field to produce a significant amount of heat in cancer cells. Depending on the temperature produced and the heating time, the death of cancer cells or their sensitivity to radiotherapy or chemotherapy is directly observed.[162]

Because nanotechnology is a fast-growing multidisciplinary field of science, it has also found application in pharmacy (Figure 34). It have been conducted studies about the route of dministration new forms of drugs or studies about the active substance of the chemical structure, what could lead to a reduce the toxicity of drug.

This technique, among others, is an innovative biodistribution method, for example, in studies on drug molecules delivered for a specific biological purpose. In recent years, interest in modern methods of drug delivery using nanostructures has increased, so you can count on a better ability to achieve a specific place of action of drugs (Tables 8–10). New excipients with potential application in drug technology have been developed, from which carriers of active substances, including proteins and genes, are constructed. The expected effect of the introduction of nanotechnology in medicine and pharmacy in this area is to increase the effectiveness of medicines and decrease the side effects of excipients (Tables 8–10). Currently, nanoparticles are mainly used as drug carriers and substances with antibacterial and virucidal

Figure 28 Some examples of dextrins.

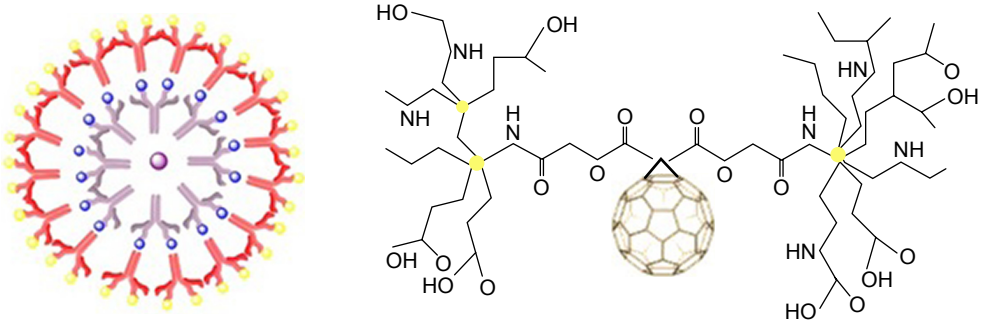

Figure 29 Structure of dendrimers.
Note: Data from Brettreich and Hirsch.[132]

properties. They also play a large role in diagnostics, where they are used in immunohistochemistry, genetic research and in the detection of pathogens and tumors. They increase the speed, accuracy and sensitivity of biological tests with small sample volumes. Despite many advantages and applications not only in the field of medicine, but also in environmental protection and in various technological branches, it is necessary to conduct the cytotoxicity tests of the nanoparticles and nanomaterials.

Fullerenes and CNTs

Fullerenes are nanostructures with a shape similar to the sphere composed of conjugated rings consisting of five or six carbon atoms. The most popular ones are 60-atom nanostructures with the shape of a truncated icosahedron. CNTs assume the shape of an empty cylinder made of coiled graphene (Figure 35). They can create structures with a length of a few centimeters and a diameter of a few nanometers. Due to the number of layers building the wall of the nanotube, they are divided into single-wall nanotubes and polyhedral nanotubes (Figures 35 and 36).

CNTs are used as drug carriers which enables their continuous and constant dosing in pathological cells (Figure 36). In addition, they may contain antibodies or enzymes specifically targeting their action.[199] For example, polyhedral nanotubes containing cisplatin show anticancer activity by inhibition of tumor cell growth.[200] Similar results were obtained by combining doxorubicin with CNTs in the treatment of breast cancer[201] or by combining carboplatin with CNTs in the treatment of bladder cancer.[202] CNTs are

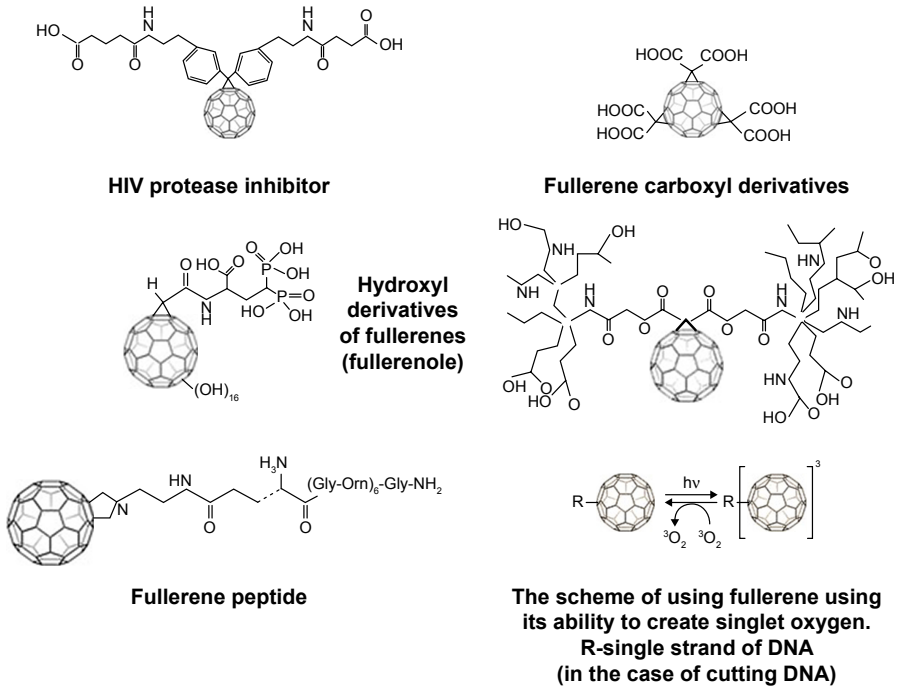

Figure 30 Dendrimers and fullerene derivatives.

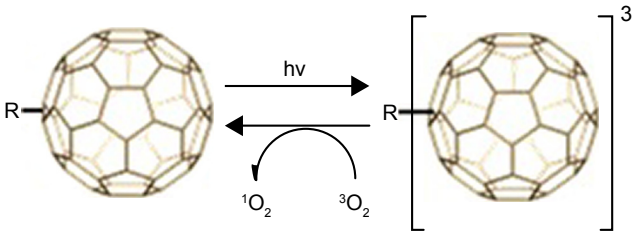

Figure 31 The scheme of fullerene using its ability to create singlet oxygen.
Notes: In the figure, symbol R means single strand of DNA (in the case of DNA cleavage). First, $^3C_{60}$ (100% efficiency) is created as a result of photoexcitation. Next, with the participation of excited fullerene and molecular oxygen, singlet oxygen $^1O_2$ is generated, while the excited fullerene returns to the ground state. As a result, the DNA strand may be cut, thanks to the action of $^1O_2$.

characterized by high semiconductivity, strong fluorescence and Raman scattering. They can also be used as a scaffold for immobilizing biomolecules. Such scaffolds are used in biological diagnostics as nanosensors in protein microarrays with a detection sensitivity up to 1 fmol/L.[203] The use of the biosensor may be based on the sensing of changes in glucose concentration in the intercellular fluid, which, as a result of the increase in the amount of sugar in the body, increases the fluorescence of the infrared nanotubes.[204] Fullerenes are used for imaging of tumors during surgical procedures and for observation of lymph nodes located closest to tumor foci. Additionally, radioactive isotopes used in radiotherapy can be introduced into the interior of nanostructures.[205]

Drug delivery nanostructures

"Drug delivery" is an interdisciplinary field of nanobiotechnology that combines engineering, biology, chemistry and medicine. This new trend of science creates the possibility of directing and releasing traditional medicines in a controlled, specific and local way. Thanks to the nanomolecules, the kinetic release of drugs could be regulated, their biodistribution adjusted and the toxic side effects minimized, while the therapeutic effect of a given drug is increased. Because the current drug delivery is characterized by a limited therapeutic due to the inability to achieve high drug concentration in the tissue and and due to the inability to direct the drug to a single cell, that's why is planned to build a generation of functional biosensors that can be controlled from the outside and that allows for "intelligent" drug delivery. The constructive goal of the nanodrug is to overcome the inherent limitations of biomacromolecular therapeutic agents, including short plasma half-life, poor stability, potential immunogenicity and maximization of therapeutic activity, while minimizing the toxic side effects of the drugs. During working on small objects, a very important feature is observed, that is, increasing the surface to volume ratio. Only this one feature gives the possibility of reducing the drug to the absolute minimum, while maintaining the therapeutic effect of the drug and also minimizing the toxic effects of the drug. The size range in nanometers increases the ability of drug delivery carriers to penetrate the cell membranes, reduces the risk of unwanted hepatic or spleen removal from the body and minimizes their uptake by the reticuloendothelial system.

Thus, the following studies[206–220] set out a new trend in scientific research "drug delivery", which consists of three thematic components:

- the properties of fullerenes described above,[8–20,206]
- design,[206–210,212–214]
- docking of drugs and molecular dynamics.[215–219]

Commercial nanoparticles

Recently, the main goal of research is to create multifunctional nanoparticles and nanomaterials, the properties of which could be controlled in the body through the local environment and external factors such as the external magnetic field. Many pharmaceutical companies have their own research programs aimed at introducing new products based on nanoparticles and nanomaterials and improving current pharmaceuticals. As a result of intense and long analyses, commercial nanosubstances have been introduced, which have been used, among others, in the diagnosis or treatment of neoplastic diseases (Table 11).

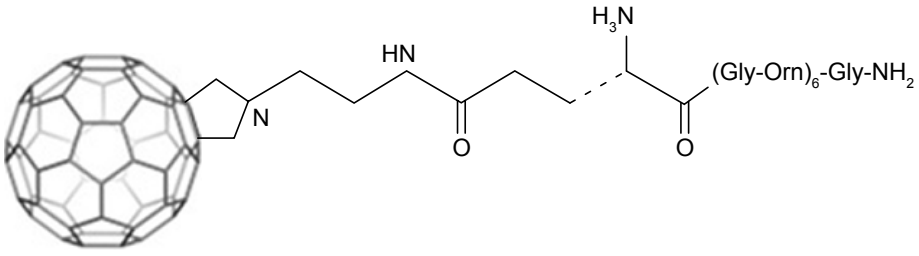

Figure 32 An analogous peptide lacking the fullerene part.

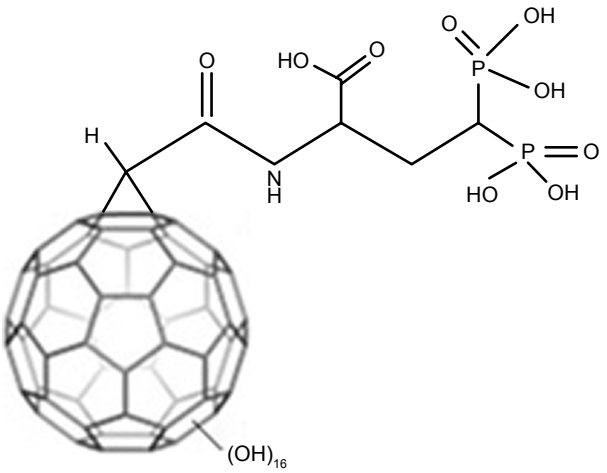

Figure 33 Diphosphate fullerene $C_{60}(OH)_{16}$AMBP.

Nanoparticles are a hope in the development of personalized medicine, not only for therapeutic purposes, that is, in real-time cancer treatment at the molecular level, but also for monitoring treatment. For anticancer treatments and molecular MRI, multifunctional and multilayered graphene-encapsulated magnetic nanoparticles were designed and developed at the same time. By assembling polymeric nanogel polyethylenimine (PEI)[216] (Acknowledgment section) and antibodies on the nanomolecule,[220] it could be possible to identify a new cancer by recognizing integrin receptors on lung cancer tissues (Figure 37).

The attached monoclonal antibody was directed to selected receptors of the integrin of tissues and tumor vessels,

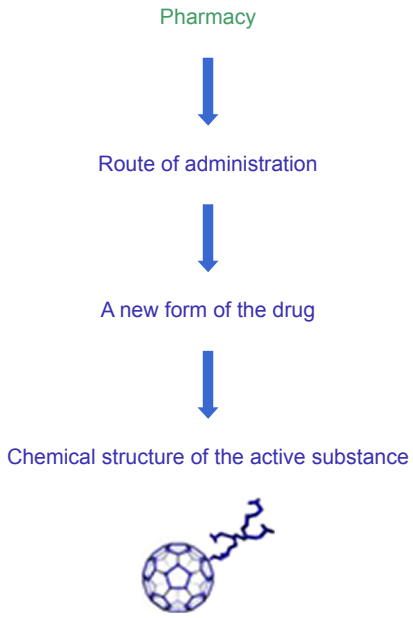

Figure 34 Application of nanostructures in pharmacy.

Table 8 Nanoparticles as carriers of anticancer drugs

Type of nanoparticle	Disease
Liposomes	Acute lymphatic leukemia,[163] ovarian cancer,[164] lung cancer[165]
Polymeric micelles	Colon cancer,[166] breast cancer,[167] lung cancer[168,169]
Dendrimers	Ovarian cancer,[170] lung cancer[171,172]
Carbon nanoparticles	Bladder cancer,[173,174] prostate cancer,[175] lung cancer,[176] breast cancer[177]
Inorganic nanoparticles	Prostate cancer,[178] osteosarcoma,[179] lung cancer,[180] malignant melanoma[181]

which was further used in reducing certain signals of transduction due to the selected functions of molecular receptors. To support the anticancer effect, the enzyme (GOx, 3QVR) was released,[220] which resulted in the reduction of ATP/ADP synthesis, that, in turn, caused hypoxia of cancerous tissues (Figure 38).

The release of the adsorbed enzyme on nanostructures was fully controlled to promote antitumor activity. Release of the enzyme, resulting in abnormal ATP/ADP synthesis, triggered hypoxic states in lung cancer cells and tissues at the molecular level. In the next step, radiotherapy was applied to target lung cancer. The studies were preceded by quantitative structure-activity relationship studies, microfluidic and genetic/epigenetic approaches to characterize multifunctional and multilayered graphene as a new drug and contrast candidate (drug delivery).

The nature of interactions between PEI[216,217] (Acknowledgment section) and GOx 3QVR[220] enzyme was studied by docking and molecular dynamics procedures. GOx is an enzyme which plays the role of biosensors that can be immobilized onto different nanomaterials and polymers such as PEI.

In order to solve the problem of maintaining the native GOx enzyme (3QVR; Figures 38 and 40) activity despite its immobilization on the surface of the PEI polymer, molecular dynamics studies were carried out (Figure 39). The stability of the complex ligand–enzyme in terms of structure and energy was assessed. Before molecular dynamics, in order to

Table 9 The use of nanoparticles in the diagnostic imaging of tumors

Picture technique	Type of nanoparticle
Computer tomography	Inorganic nanoparticles[182]
MRI	Magnetic nanoparticles[183,184]
Positron emission tomography	Silicon nanoparticles[185]
Photoacoustic imaging	Carbon nanoparticles[186,187]

Table 10 The use of nanoparticles in the diagnostic imaging of tumors

Method of treatment	Type of nanoparticle	Disease
Photodynamic therapy	Inorganic nanoparticles	Breast cancer,[188] liver cancer[189]
	Carbon nanoparticles	Liver cancer,[190] breast cancer[191]
Photothermal therapy	Magnetic nanoparticles	Prostate cancer,[192] glioblastoma multiforme[193]
	Inorganic nanoparticles	Squamous cell carcinoma of the skin[194,195]
	Carbon nanoparticles	Breast cancer,[196] neuroma[197]
Gene silencing	Inorganic nanoparticles	Liver cancer[198]

search the best PEI–GOx affinity, docking had been carried out, after which the structure of PEI[216,217] (Acknowledgment section) was selected (C14N8_07_B22; Figure 39). Two places with the best affinity were found after docking (Figure 40), inside of GOx (LIG1) and on its surface (LIG2).

These ligand–enzyme complexes showed differences in their structural and energetic characteristics (see Acknowledgment section).[216,217]

The RMSD values of systems, their average values and SDs showed that these two systems (LIG1 and LIG2; Figure 41) were quite similar. In the first active side, inside of the protein, the stabilization of RMSD ligand appeared with values with small deviations 0.4 Å after 20 ns, while in case of complex formed by ligand on the surface of enzyme, the deviation of RMSD values reached much more higher values (Figure 41).

In the first case, small deviation of RMSD values means possibilities of strong and medium hydrogen bond formation, and in the second case, it means possibilities of weak hydrogen bond formation. The mobility of the LIG1, as we can see in Figure 42, is correlated with changes in the values of dihedral angle (C7–N3–C4–C3), and going further, its structural property decides about hydrogen bond forces.

Inside of the protein, the hydrogen bonds (ie, interactions) formed between enzyme and ligand were shorter and stronger, while the lengths of the hydrogen bonds of ligand–enzyme created on the surface of protein were long and weak (Figure 43).

Because one of the problems in creation of intelligent nanoparticle was immobilization of enzyme on the polymer surface, the study of immobilization of GOx on PEI was carried out during molecular dynamics. The analysis of trajectories confirmed energetic and structural stabilization of the formed ligand–enzyme complexes inside of the protein and on its surface.

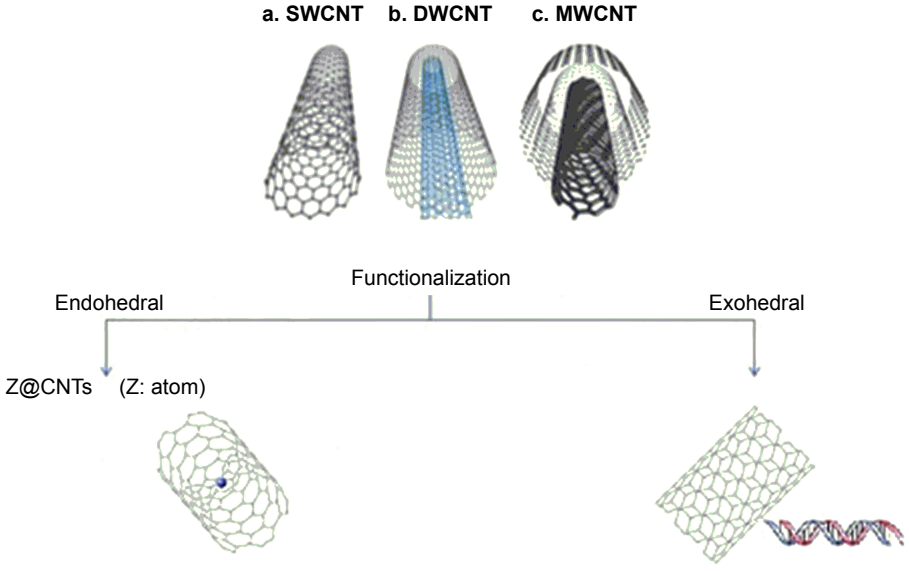

Figure 35 CNTs.[199–205]
Abbreviations: CNTs, carbon nanotubes; DWCNT, double-walled carbon nanotube; MWCNT, polyhedral carbon nanotube; SWCNT, single-walled carbon nanotube.

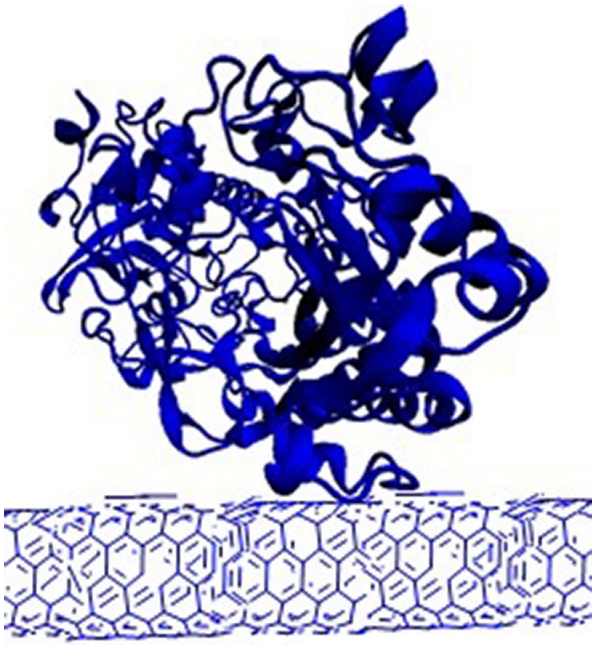

Figure 36 Equilibrated structure of the SWNT–PSE–GOX complex.[199]
Note: Data from Mackay.[199]
Abbreviation: SWNT, single-walled nanotube.

Conclusion and future perspectives

There are several reasons why nanotechnology is currently taking the lead among the most intensively developing research trends. Nano-matter often exhibits new properties, other than those of the morphology of a continuous solid. Also, new phenomena appear at the nanoscale, which are unknown in the case of microcrystalline objects. For this reason, nanomaterials have already found numerous applications,

Table 11 Commercial uses of nanoparticles in medicine

Nanoparticles	Application
Gold nanoparticles	Diagnosis of HIV (in vitro)
	Diagnosis of blood vessels
	Probes in PCR, Western blot
Silver nanoparticles	Bandages ACTICOAT
	Signal amplifier
Nanoparticles of apatite	Toothpastes
Magnetic nanoparticles	Cancer diagnostics (in vitro)
	Cell recognition
	Diagnosis and treatment of cardiovascular diseases
Quantum dots	Probes in Western blot
	Bio-detection
	Flow cytometry
	Luminescent biomarkers
Carbon nanotubes	Diagnosis of the respiratory system
Dendrimers	Treatment of HIV, cancer and inflammation

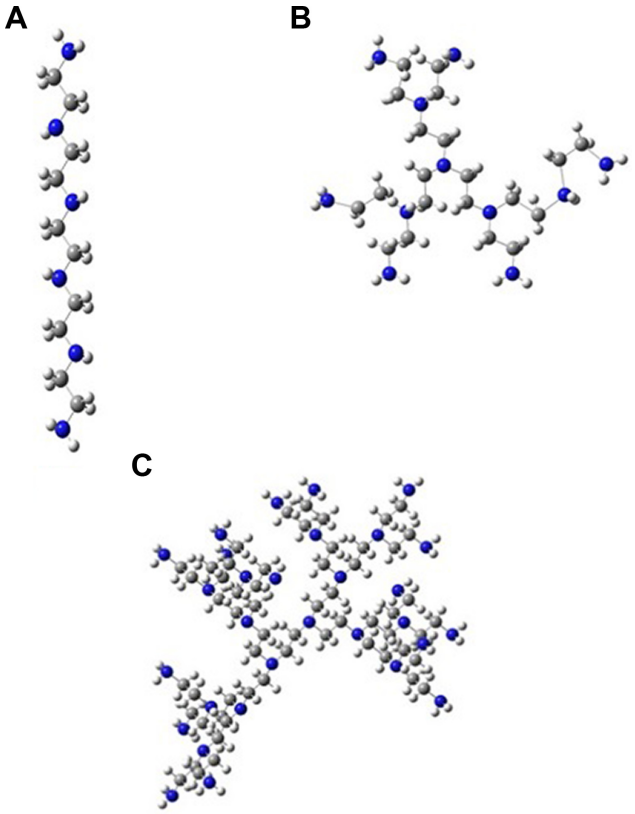

Figure 37 Examples of polyethylenimine molecules: linear (**A**); branched (**B**) and dendrimer (**C**).[216,217*]
Note: Data from Szefler et al.[216,217]

which have been described in this review. Among intensively developed various branches of nanotechnology, nanomedicine stands out particularly.[222] It uses nanoparticles (NCz) and nanomaterials in areas such as nanodiagnostics, nanopharmacology and nanooncology. Nanodiagnostics is mainly based on rapid diagnosis of disease states by using NCz as markers and indicators in diagnostic tests. But one of the best

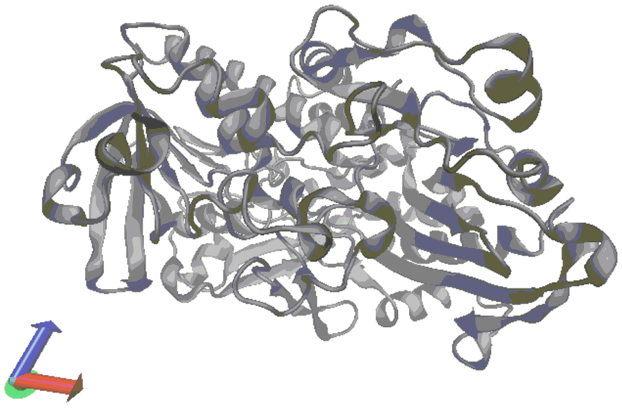

Figure 38 The protein 3QVR.[216*,217*,220]

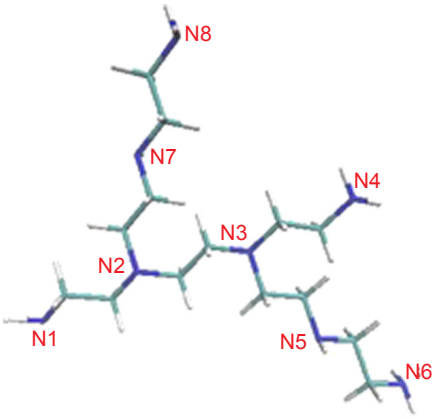

Figure 39 The ligand PEI_C14N8_07_B22.[216*,217*]

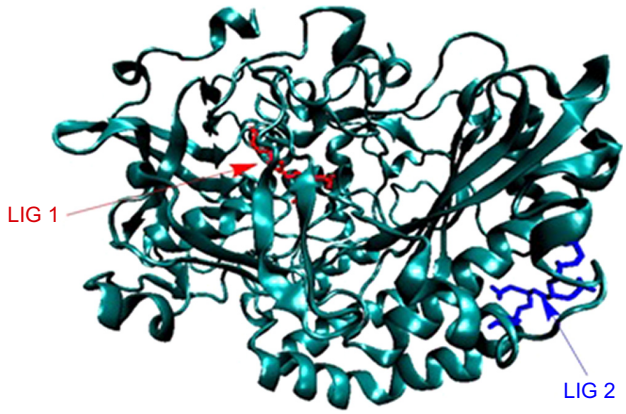

Figure 40 Two sites of the interaction PEI_C14N8_07_B22–3QVR were used during molecular dynamics: inside (LIG1) and on its surface (LIG2).
Note: Data from et al[216] and Szefler et al.[217]

developing areas of nanomedicine is nanopharmacology.[221] Thanks to the use of nanoparticles, the pharmacodynamic and pharmacokinetic parameters of the drug are improved, including, among others, bioavailability, time of release of the active substance and prolongation of pharmacological action time. For therapeutic purposes, nanoparticles in the form of liposomes, fullerenes, nanotubes and dendrimers are most commonly used.[222] Therefore, nanopharmacology is based on the creation of carrier nanosystems enabling the selective delivery of the drug and its controlled release in pathological cells or tissues. Nanopharmacology also deals with the creation of new nanodrugs and the improvement of existing ones.[223] Therefore, the introduction of nanotechnology into medicine and pharmacology opens new possibilities for the development of these disciplines, gives great hope for the creation of drugs where toxicological properties are reduced to a minimum, reduces the doses of medicines, offers targeted treatment, that is, getting the medicines exactly to diseased areas and, at the same time, protecting healthy tissues. It also increases diagnostic possibilities, is an intraoperative assistant for doctors and provides the opportunity to quickly convalesce patients by minimizing the invasiveness of treatments. Such creation of new "nanodrugs" requires a special understanding of the properties of nanoparticles. That is why, in this article, the way of creating a new nanodrug has been described from ab initio calculations by docking and molecular dynamic applications, up to creation of new nanodrug, as a proposition which can be used in the near

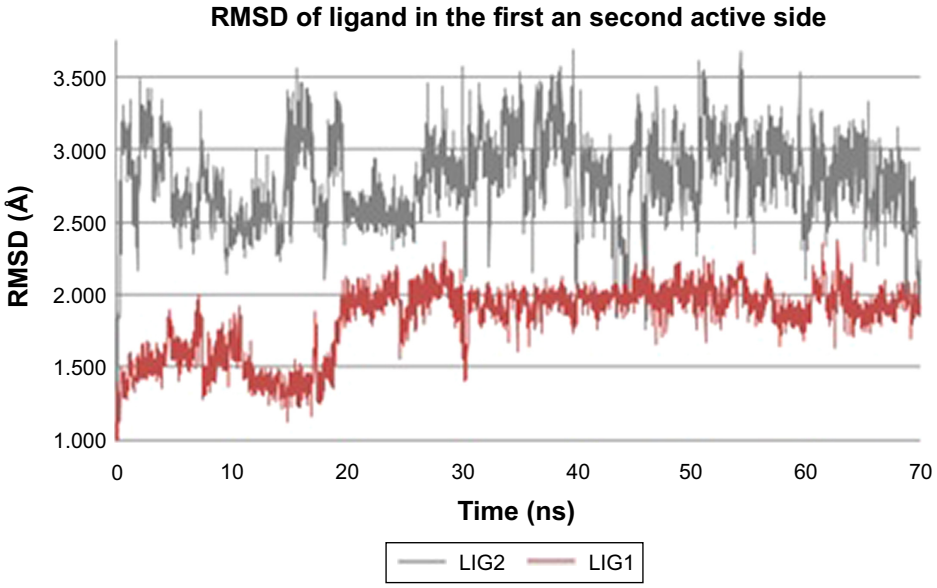

Figure 41 RMSD distribution of ligand PEI_C14N8_07_B22 inside of protein and on the protein surface.
Abbreviation: RMSD, root-mean-square deviation.

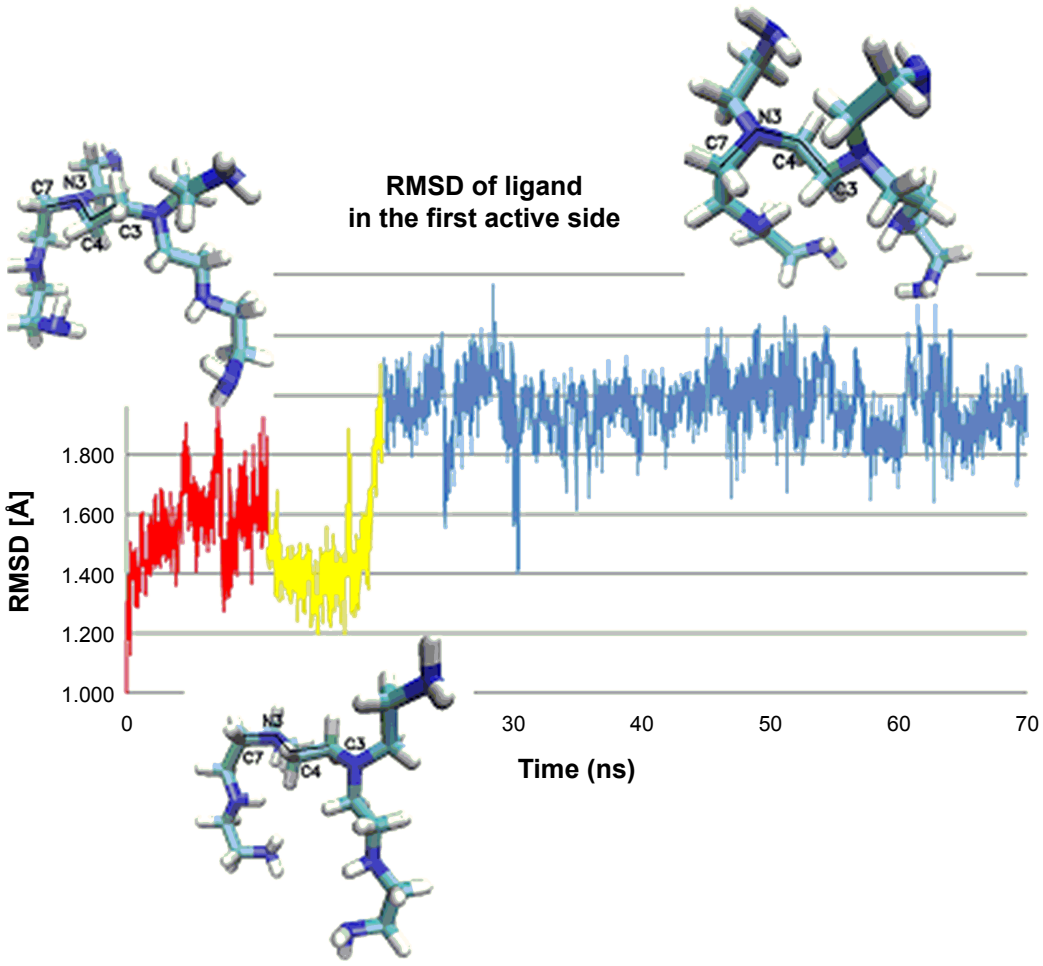

Figure 42 Distribution of values of the dihedral angle of ligand (C7–N3–C4–C3, LIG1) during MD simulation inside of the protein.
Abbreviation: RMSD, root-mean-square deviation.

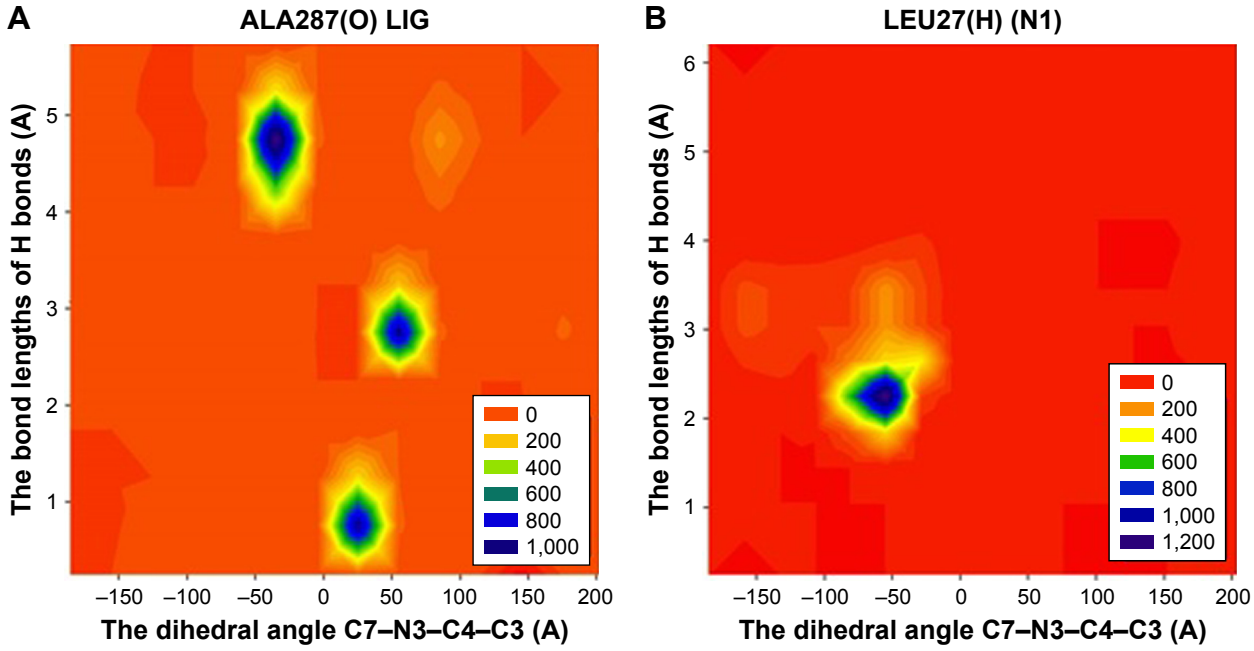

Figure 43 (*Continued*)

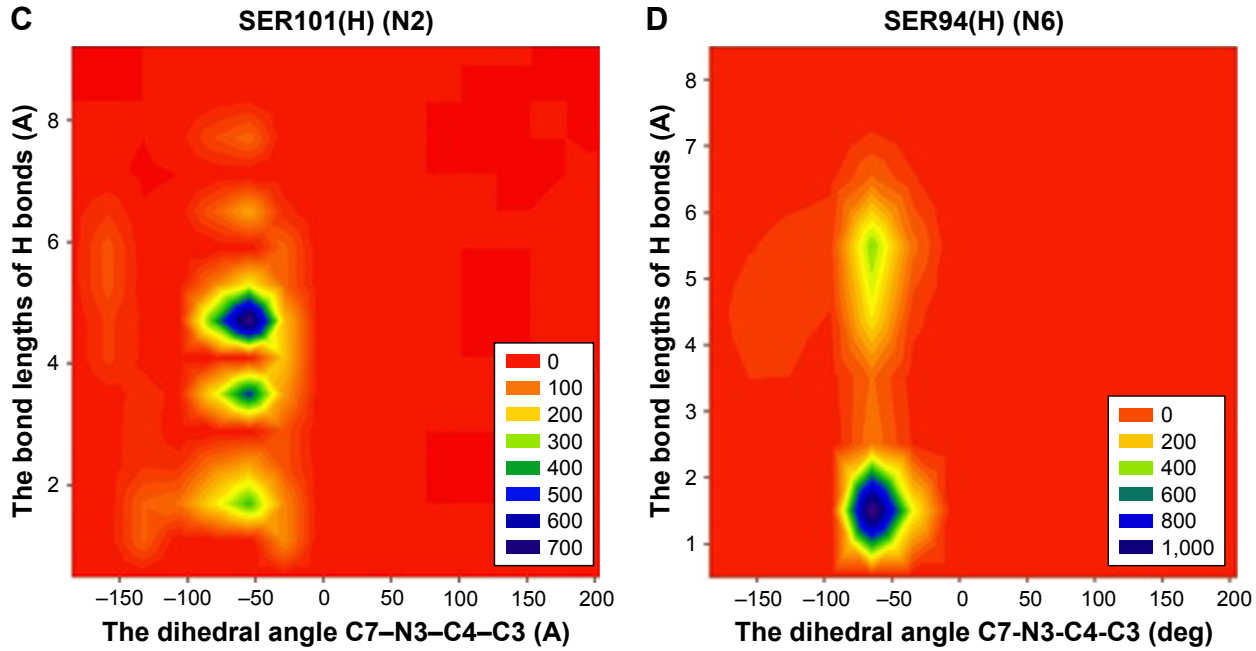

Figure 43 The length of hydrogen bonds created inside of protein (LIG1) as a function of dihedral angle C_7–N_3–C_4–C_3 during MD simulation.
Notes: (**A**) The length of hydrogen bonds created between oxygen atom (O) of aminoacid Alanine 287 (ALA287) and ligand. (**B**) The length of hydrogen bonds created between hydrogen atom (H) of aminoacid Leucine 27 (LEU27) and nitrogen atom N1 of ligand. (**C**) The length of hydrogen bonds created between hydrogen atom (H) of aminoacid Serine 101 (SER101) and nitrogen atom N2 of ligand. (**D**) The length of hydrogen bonds created between hydrogen atom (H) of aminoacid Serine 94 (SER94) and nitrogen atom N6 of ligand.

future in personalized medicine. Nanotechnology is the source of a great revolution in medicine. It gives great hope for better and faster treatment of many diseases, and thus gives hope for a better tomorrow.

Acknowledgments

This review is dedicated to Professor MV Diudea, as a thanks for fruitful cooperation for many years. Some research forming a part of this review was conducted and financed as part of an international project entitled "Self-navigated integrin receptors seeking thermally-smart multifunctional few-layer graphene-encapsulated magnetic nanoparticles for molecular MRI-guided anticancer treatments in real time personalized nanomedicine (acronym GEMNS)": The European Union's Seventh Framework Program ERA-NET EuroNanoMed II (European Innovative Research and Technological Development Projects in Nanomedicine). This research was supported by PL-Grid Infrastructure.

Disclosure

The author reports no conflicts of interest in this work.

References

1. "Robert F. Curl Jr. – Biographical". *Nobelprize.org*. Available from: https://www.nobelprize.org/prizes/chemistry/1996/curl/auto-biography. Accessed July 19, 2016.
2. Kroto HW, Heath JR, O'Brien SC, Curl RF, Smalley RE. C60: Buckminster fullerene. *Nature*. 1985;318(6042):162–163.
3. Krätschmer W, Lamb LD, Fostiropoulos K, Huffman DR. Solid C60: a new form of carbon. *Nature*. 1990;347(6291):354–358.
4. Stolnik S, Illum L, Davis SS. Long circulating microparticulate drug carriers. *Adv Drug Deliv Rev*. 1995;16(2–3):195–214.
5. Ogawara K-I, Yoshida M, Furumoto K, et al. Uptake by hepatocytes and biliary excretion of intravenously administered polystyrene microspheres in rats. *J Drug Target*. 1999;7(3):213–221.
6. Xie Q, Perez-Cordero E, Echegoyen L. Electrochemical detection of C606- and C706-: enhanced stability of fullerides in solution. *J Am Chem Soc*. 1992;114(10):3978–3980.
7. Kolmakov A, Moskovits M. Chemical sensing and catalysis by one-dimensional metal-oxide nanostructures. *Annu Rev Mater Res*. 2004;34(1):151–180.
8. Szefler B, Diudea MV. On molecular dynamics of the diamond D5 seeds. *Struct Chem*. 2012;23(3):717–722.
9. Szefler B, Ponta O, Diudea MV. Energetics of polybenzene multi-tori. *J Mol Struct*. 2012;1022:89–93.
10. Szefler B, Diudea MV. Polybenzene multitori. *Central Eur J Med*. 2012;7(6):1779–1785.
11. Szefler B, Diudea M. Modeling tetrapodal nanotube junctions. *Comput Methods Sci Technol*. 2012;18(2):111–115.
12. Diudea MV, Szefler B. Nanotube junctions and the genus of multi-tori. *Phys Chem Chem Phys*. 2012;14(22):8111–8115.
13. Szefler B, Saheli M, Diudea MV. Sumanene units in P-type surface networks. *Acta Chim Slov*. 2012;59:177–182.
14. Diudea MV, Szefler B. Omega polynomial in polybenzene multi tori. *Iran J Math Sci Inform*. 2012;7(2):75–82.
15. Szefler B, Diudea MV. Polybenzene revisited. *Acta Chim Slov*. 2012;59:795–802.
16. Szefler B. On molecular dynamics of the diamond D_5 substructures. In: Diudea MV, Nagy CL, editors. *Carbon Materials: Chemistry and Physics, 6: Diamond and Related Nanostructures*. New York: London: Springer, Dordrecht, Heidelberg; 2013:119–137.
17. Szefler B, Diudea MV. Quantum-mechanical calculations on molecular substructures involved in nanosystems. *Molecules*. 2014;19(10):15468–15506.

18. Diudea MV, Szefler B. Topology of C20 based spongy nanostructures. *Comput Methods Sci Technol*. 2015;21(2):65–68.
19. Diudea MV, Szefler B, Nagy CL, Bende A. Exotic allotropes of carbon. In: Puts MV, Ori O, editors. *Exotic Properties of Carbon Nanomatter*. New York: London: Springer, Dordrecht Heidelberg; 2015: 185–201.
20. Szefler B, Diudea MV. Cluj and omega polynomials in PAHs and fullerenes. *Rev Curr Org Chem Bentham Publ*. 2015;19(4):311–330.
21. Dubois D, Kadish KM, Flanagan S, Haufler RE, Chibante LPF, Wilson LJ. Spectroelectrochemical study of the C_{60} and C_{70} fullerenes and their mono-, di-, tri- and tetraanions. *J Am Chem Soc*. 1991;113(11): 4364–4366.
22. Przygocki W, Włochowicz A. Fulereny i nanorurki [Fullerenes and nanotubes. Properties and application]. Wydaw. Nauk.-Techn., Warszawa; 2001. Polish.
23. Jones DEH. The concept of hollow molecules made from graphite-like sheets was suggested in remarkably inventive piece by David E.H Jones in his column "Ariadne" in the New Scientist magazine. *New Scientist*. 1966;32:245.
24. Heath JR, Zhang Q, O'Brien SC, Curl RF, Kroto HW, Smalley RE. The formation of long carbon chain molecules during laser vaporization of graphite. *J Am Chem Soc*. 1987;109(2):359–363.
25. Stevenson S, Rice G, Glass T, et al. Erratum: Small-bandgap endohedral metallofullerenes in high yield and purity. *Nature*. 1999;401(6748): 55–57.
26. Feng L, Sun B, He X, Gu Z. Isolation and spectroscopic study of a series of monoterbium endohedral metallofullerenes. *Fuller Nanotub Car N*. 2002;10(4):353–361.
27. Guo T, Smalley RE, Scuseria GE. Ab initio theoretical predictions of C28, C28H4, 28F4, (Ti@ C28) H4, and M@ C28 (M=Mg, Al, Si, S, Ca, Sc, Ti, Ge, Zr, and Sn). *J Chem Phys*. 1993;99(1):352–359.
28. Talberg HJ. The crystal structure of magnesium p-nitrosophenolate. Hexahydrate. The Influence of hydrogen bonding on conjugation in the p-nitrosophenolate ion. *Acta Chem Scand*. 1977;A(31):37–46.
29. Talberg HJ. The crystal and molecular structure of sodium p-nitrosophenolate trihydrate. *Acta Chem Scand A*. 1975;29:10.
30. Katritzky AR, Karelson M, Wells AP. Aromaticity as a quantitative concept. 6. Aromaticity variation with molecular environment. *The Journal of organic chemistry*. 1996;61(5):1619–1623.
31. Feixas F, Matito E, Poater J, Sola M. Electron sharing indexes at the correlated level. Application to aromaticity calculations. *J Comput Chem*. 2008;29:1543–1554.
32. Balaban AT. Is aromaticity outmoded? *Pure Appl Chem*. 1980;52(6): 1409–1429.
33. Poater J, Garcıa-Cruz I, Illas F, Solá M. Discrepancy between common local aromaticity measures in a series of carbazole derivatives. *Chem Phys*. 2004;6:314–318.
34. Krygowski TM, Cyrañski MK, Czarnocki Z, Häfelinger G, Katritzky AR. Aromaticity: a theoretical concept of immense practical importance. *Tetrahedron*. 2000;56(13):1783–1796.
35. Minkin VI, Glukhovtsev MN, Simkin BY. *Aromaticity and Antiaromaticity, Aromaticity and Antiaromaticity. Electronic and Structural Aspects*. New York: John Wiley & Sons. Inc.; 1994.
36. Maksić ZB, Vianello R. Quest for the origin of basicity: initial vs final state effect in neutral nitrogen bases. *J Phys Chem A*. 2002;106(2): 419–430.
37. Balaban AT, Oniciu DC, Katritzky AR. Aromaticity as a cornerstone of heterocyclic chemistry. *Chem Rev*. 2004;104(5):2777–2812.
38. Poater J, Duran M, Solà M, Silvi B. Theoretical evaluation of electron delocalization in aromatic molecules by means of atoms in molecules (AIM) and electron localization function (ELF) topological approaches. *Chem Rev*. 2005;105(10):3911–3947.
39. Flygare WH. Magnetic interactions in molecules and an analysis of molecular electronic charge distribution from magnetic parameters. *Chem Rev*. 1974;74(6):653–687.
40. Dauben HJ, Wilson JD, Laity JL. Diamagnetic susceptibility exaltation as a criterion of aromaticity. *J Am Chem Soc*. 1968;90(3):811–813.
41. Dauben HJ, Wilson JD, Laity JL. Diamagnetic susceptibility exaltation in hydrocarbons. *J Am Chem Soc*. 1969;91(8):1991–1998.
42. Dauben HJ, Wilson JD, Laity JL. *Nonbenzoid Aromaticity*. Snyder JP, editor. Elsevier, Academic Press, INC, New York, New York. United Kingdom Edition published by ACADEMIC PRESS, INC. (LONDON) LTD, London. 1971;2.
43. Krygowski TM, Cyrański M, Ciesielski A, Świrska B, Leszczyński P. Separation of the energetic and geometric contributions to aromaticity. 2. Analysis of the aromatic character of benzene rings in their various topological environments in the benzenoid hydrocarbons. Crystal and molecular structure of coronene. *J Chem Inf Comput Sci*. 1996;36(6):1135–1141.
44. Lazzeretti P. Ring currents. *Prog Nucl Magn Reson Spectrosc*. 2000; 36(1):1–88.
45. Howard ST, Krygowski TM. Benzenoid hydrocarbon aromaticity in terms of charge density descriptors. *Can J Chem*. 1997;75(9): 1174–1181.
46. Krygowski TM, Cyrański M. Separation of the energetic and geometric contributions to the aromaticity. Part IV. A general model for the π-electron systems. *Tetrahedron*. 1996;52(30):10255–10264.
47. Krygowski TM. Crystallographic studies of inter- and intramolecular interactions reflected in aromatic character of .pi.-electron systems. *J Chem Inf Model*. 1993;33(1):70–78.
48. Cysewski P, Szefler B, Szatyłowicz H, Krygowski TM. An explicit solvent quantum chemistry study on the water environment influence on the interactions of fluoride with phenol. *New J Chem*. 2009;33(4): 831–837.
49. Krygowski TM, Cyrański MK. Structural aspects of aromaticity. *Chem Rev*. 2001;101(5):1385–1420.
50. Katritzky AR, Karelson M, Sild S, Krygowski TM, Jug K. Aromaticity as a quantitative concept. 7. Aromaticity reaffirmed as a multidimensional characteristic. *J Org Chem*. 1998;63(15):5228–5231.
51. Palusiak M, Krygowski TM. Application of AIM parameters at ring critical points for estimation of π-electron delocalization in six-membered aromatic and quasi-aromatic rings. *Chemistry*. 2007;13(28): 7996–8006.
52. Cyrański MK, Ciesielski A, Krygowski TM, Stępień DK. Application of graph theory and topological models for the determination of fundamentals of the aromatic character of pi-conjugated hydrocarbons. *Pure Appl Chem*. 2012;84(4):1069–1088.
53. Kadish KM, Ruoff RS. *Fullerenes: Chemistry, Physics, and Technology*: John Wiley & Sons; 2000.
54. Diudea MV, Nagy CL. *Periodic Nanostructures*. The Netherlands: Springer. Dordrecht; 2007.
55. Diudea MV. *Nanostructures*. *Novel Architecture*. Diudea MV, editor. Nova: New York, NY, USA: 2005.
56. Diudea MV. *Nanomolecules and Nanostructures-Polynomials and Indices*. *MCM Series 10*. Kragujevac. Serbia: University of Kragujevac Press; 2010.
57. Amsharov KY, Jansen M. A C78 fullerene precursor: toward the direct synthesis of higher fullerenes. *J Org Chem*. 2008;73(7):2931–2934.
58. Amsharov K, Jansen M. Synthesis of a higher fullerene precursor – an "unrolled" C84 fullerene. *Chem Commun (Camb)*. 2009;347(19): 2691–2693.
59. Barborini E, Piseri P, Milani P, Benedek G, Ducati C, Robertson J. Negatively curved spongy carbon. *Appl Phys Lett*. 2002;81(18): 3359–3361.
60. Terrones H, Mackay AL. From C60 to negatively curved graphite. Progress in crystal growth and characterization of materials. 1997;34(1–4):25–36.
61. Fowler PW, Pisanski T. Leapfrog transformations and polyhedra of Clar type. *J Chem Soc Faraday Trans*. 1994;90(19):2865–2871.
62. Schleyer P, Maerker C, Dransfeld A, Jiao H, van Eikema Hommes NJR. Nucleus-independent chemical shifts: a simple and efficient aromaticity probe. *J Am Chem Soc*. 1996;118(26):6317–6318.
63. Pop R, Medeleanu M, Diudea M, Szefler B, Cioslowski J. Fullerenes patched by flowers. *Open Chem*. 2013;11(4):527–534.

64. Diudea MV. Diamond D5, a novel allotrope of carbon. *Stud Univ Babes-Bolyai Chem*. 2010;55(4):11–17.
65. Nagy K, Nagy CL, Tasnadi E, Katona G, Diudea MV. Hyper-diamonds and dodecahedral architectures by tetrapodal carbon nanotube junctions. *Acta Chim Slov*. 2013;60(1):1–4.
66. Diudea MV. *Nanostructures, Novel Architecture*. New York, NY: NOVA; 2005.
67. Decarli PS, Jamieson JC. Formation of diamond by explosive shock. *Science*. 1961;133(3467):1821–1822.
68. Aleksenskii AE, Baidakova MV, Vul' AY, Davydov VY, Pevtsova YA. Diamond–graphite phase transition in ultradisperse-diamond clusters. *Phys Solid State*. 1997;39(6):1007–1015.
69. Ōsawa E. Recent progress and perspectives in single-digit nanodiamond. *Diam Relat Mater*. 2007;16(12):2018–2022.
70. Ōsawa E. Monodisperse single nanodiamond particulates. *Pure Appl Chem*. 2008;80(7):1365–1379.
71. Williams OA, Douhéret O, Daenen M, Haenen K, Ōsawa E, Takahashi M. Enhanced diamond nucleation on monodispersed nanocrystalline diamond. *Chem Phys Lett*. 2007;445(4–6):255–258.
72. Dubrovinskaia N, Dub S, Dubrovinsky L. Superior wear resistance of aggregated diamond nanorods. *Nano Lett*. 2006;6(4):824–826.
73. Khachatryan AK, Aloyan SG, May PW, Sargsyan R, Khachatryan VA, Baghdasaryan VS. Graphite-to-diamond transformation induced by ultrasound cavitation. *Diam Relat Mater*. 2008;17(6):931–936.
74. Frondel C, Marvin Ub. Lonsdaleite, a hexagonal polymorph of diamond. *Nature*. 1967;214:587–589.
75. Diudea MV, Bende A, Janežič D. Omega polynomial in diamond-like networks. *Fuller Nanotub Car N*. 2010;18(3):236–243.
76. Hyde ST, O'Keeffe M, Proserpio DM. A short history of an elusive yet ubiquitous structure in chemistry, materials, and mathematics. *Angew Chem Int Ed Engl*. 2008;47(42):7996–8000.
77. Diudea MV, Ilíc A. All-pentagonal face multi tori. *J Comput Theor Nanosci*. 2011;8(4):736–739.
78. Diudea MV, Petitjean M. Symmetry in multi tori. *Symmetry Cult Sci*. 2008;19(4):285–305.
79. Gund P, Gund TM. How many rings can share a quaternary atom? *J Am Chem Soc*. 1981;103(15):4458–4465.
80. Paquette LA, Vazeux M. Threefold transannular epoxide cyclization. Synthesis of a heterocyclic 17-hexaquinane. *Tetrahedron Lett*. 1981; 22(4):291–294.
81. Kuck D. A facile route to benzoannelated centrotriquinanes. *Angew Chem Int Ed Engl*. 1984;23(7):508–509.
82. Kuck D, Schuster A, Paisdor B, Gestmann D. Benzoannelated centropolyquinanes. Part 21. Centrohexaindane: three complementary syntheses of the highest member of the centropolyindane family. *J Chem Soc Perkin Trans 1*. 1995;6:721–732.
83. Kuck D. Three-dimensional hydrocarbon cores based on multiply fused cyclopentane and indane units: centropolyindanes. *Chem Rev*. 2006;106(12):4885–4925.
84. Szefler B, Diudea MV. Spongy nanostructures. *J Nanosci Nanotechnol*. 2017;17(1):323–328.
85. Delgado-Friedrichs O, Foster MD, O'Keeffe M, Proserpio DM, Treacy MMJ, Rigid YOM. Flexible and impossible zeolite and related structures. *J Solid State Chem*. 2005;178:2533–2554.
86. Blase X, Benedek G, Bernasconi M. Structural, mechanical and superconducting properties of clathrates. *Computer-Based Modeling of Novel Carbon Systems and Their Properties*. *Beyond Nanotubes*. Colombo L, Fasolino A, editors. Chap 6. Springer; 2010:171–206.
87. O'Keeffe M, Adams GB, Sankey OF. Predicted new low energy forms of carbon. *Phys Rev Lett*. 1992;68(15):2325–2328.
88. Terrones H, Mackay AL. Triply periodic minimal surfaces decorated with curved graphite. *Chem Phys Lett*. 1993;207(1):45–50.
89. Benedek G, Vahedi-Tafreshi H, Barborini E. The structure of negatively curved spongy carbon. *Diam Relat Mater*. 2003;12(3–7):768–773.
90. Valencia F, Romero AH, Hernández E, Terrones M, Terrones H. Theoretical characterization of several models of nanoporous carbon. *New J Phys*. 2003;516:123–123.
91. Terrones H, Terrones M. Curved nanostructured materials. *New J Phys*. 2003;5(126):1–37.
92. Blase X, Benedek G, Bernasconi M. *Computer-Based Modeling of Novel Carbon Systems and Their Properties*. *Beyond Nanotubes*. Colombo L, Fa solino A, editors. Springer; 2010:171–206.
93. Diudea MV. Diamond D5, a novel allotrope of carbon. *Stud Univ Babes-Bolyai Chem*. 2010;55(4):11–17.
94. Diudea MV, CsL N, Ilić A. *Carbon Bonding and Structures*. Putz MV, editor. *Springer*. 2011:273–289.
95. Diudea MV, Nagy CL. Counting polynomials of nanostructures. In: *Periodic Nanostructures*. Dordrecht: Springer; 2007:69–114.
96. Diudea MV. *Nanostructures: Novel Architecture*. Nova Publishers; 2005.
97. Ivanovskii AL. Hyperdiamonds. *Russian J Inorganic Chem*. 2008; 53(8):1274–1282.
98. Lenosky T, Gonze X, Teter M, et al. Energetics of negatively curved graphitic carbon. *Nature*. 1992;355(6358):333–335.
99. Mackay AL, Terrones H. Diamond from graphite. *Nature*. 1991; 352(6338):762.
100. Terrones H, Mackay AL. The geometry of hypothetical curved graphite structures. In: *The Fullerenes*. 1993:113–122.
101. Schwarz HA. *Über Minimalflächen, Monatsber*. Berlin Akad., Berlin; 1865. German.
102. Schwarz HA. *Gesammelte Matematische Abhandlungen* [Collected Matematic Essays]. Berlin: Springer; 1890. German.
103. Diudea MV. *Nanomolecules and Nanostructures – Polynomials and Indices*. *MCM series*. Serbia: Univ. Kragujevac; 2010. No. 10.
104. Yaghi OM, O'Keeffe M, Ockwig NW, Chae HK, Eddaoudi M, Kim J. Reticular synthesis and the design of new materials. *Nature*. 2003;423(6941):705–714.
105. Diudea MV, John PE, Graovac A, Primorac M, Pisanski T. Leapfrog and related operations on toroidal fullerenes. *Croat Chem Acta*. 2003; 76(2):153–159.
106. Diudea MV. Covering forms in nanostructures. *Forma*. 2004;19(3): 131–163.
107. Ştefu M, Diudea MV, John PE. Composite operations on maps. *Stud Univ Babes-Bolyai Chem*. 2005;50(2):165–174.
108. Diudea MV. Nanoporous carbon allotropes by septupling map operations. *J Chem Inf Model*. 2005;45(4):1002–1009.
109. Diudea MV, Stefu M, John PE, Graovac A. Generalized operations on maps. *Croat Chem Acta*. 2006;79(3):355–362.
110. Stefu M, Diudea MV. CVNET Software ("Babes-Bolyai" University, Cluj). 2005.
111. Nagy CSL, Diudea MV. Nano Studio Software ("Babes-Bolyai" *University, Cluj)*. 2009.
112. Frisch MJ, Trucks GW, Scuseria GE, et al. Gaussian 09 Inc. Wallingford CT, Revision A.1. 2009.
113. Nagy CSL, Diudea MV. JSChem software program ("Babes-Bolyai" University, Cluj). 2005.
114. Falahati-Nezhad F, Azari M. The inverse sum indeg index of some nanotubes. *Stud Univ Babes-Bolyai Chem*. 2016;61(1).
115. Saito M, Miyamoto Y. Theoretical identification of the smallest fullerene, C 20. *Physical review letters*. 2001;87(3):035503.
116. Diudea MV. Hex tori from square tori. *Stud Univ Babes-Bolyai*. 2003;48:3–10.
117. Clar E. *Polycyclic Hydrocarbons*. London: Acad Press; 1964.
118. John PE, Vizitiu AE, Cigher S, Diudea MV. CI index in tubular nanostructures. *MATCH Commun Math Comput Chem*. 2007;57(2): 479–484.
119. Haddon RC. Rehybridization and .pi.-orbital overlap in nonplanar conjugated organic molecules: .pi.-orbital axis vector (POAV) analysis and three-dimensional Hueckel molecular orbital (3D-HMO) theory. *J Am Chem Soc*. 1987;109(6):1676–1685.
120. Haddon RC. Measure of nonplanarity in conjugated organic molecules: which structurally characterized molecule displays the highest degree of pyramidalization? *J Am Chem Soc*. 1990;112(9): 3385–3389.

121. Randić M. Aromaticity of polycyclic conjugated hydrocarbons. *Chem Rev*. 2003;103(9):3449–3606.
122. Krygowski TM, Cyrański M. *Aromaticity in Heterocyclic Compounds*. Springer; 2009.
123. Clar E. *The Aromatic Sextet*. New York: Wiley; 1972.
124. Bende A, Diudea MV. *Diamond and Related Nanostructures*. Diudea MV, Nagy CL, editors. Dordrecht: Springer; 2013:107.
125. Aradi B, Hourahine B, Frauenheim T. Self-interaction and strong correlation in DFTB. *J Phys Chem A*. 2007;111:5671–5677.
126. Elstner M, Porezag D, Jungnickel G, et al. Self-consistent-charge density-functional tight-binding method for simulations of complex materials properties. *Phys Rev B*. 1998;58(11):7260–7268.
127. Elstner M, Hobza P, Frauenheim T, Suhai S, Kaxiras E. Hydrogen bonding and stacking interactions of nucleic acid base pairs: a density-functional-theory based treatment. *J Chem Phys*. 2001;114(12):5149–5155.
128. Elstner M, Jalkanen KJ, Knapp-Mohammady M, Frauenheim T, Suhai S. DFT studies on helix formation in *N*-acetyl-(L-alanyl)$_n$-*N*′-methylamide for n=1–20. *Chem Phys*. 2000;256:15–27.
129. Elstner M, Jalkanen KJ, Knapp-Mohammady M, Frauenheim T, Suhai S. Energetics and structure of glycine and alanine based model peptides: approximate SCC-DFTB, AM1 and PM3 methods in comparison with DFT, HF and MP2 calculations. *Chem Phys*. 2001;263(2–3):203–219.
130. Andersson T, Nilsson K, Sundahl M, Westman G, Wennerstrom O. C_{60} embedded in γ-cyclodextrin: a water-soluble fullerene. *J Chem Soc Chem Commun*. 1992;8:604–606.
131. Wilson SR, Lu Q, Qy L. Electrospray MS studies of C60 Diels–Alder chemistry: characterization of a C60 Adduct with the Danishefsky Diene. *Tetrahedron Lett*. 1993;34(50):8043–8046.
132. Brettreich M, Hirsch A. A highly water-soluble dendro[60]fullerene. *Tetrahedron Lett*. 1998;39(18):2731–2734.
133. Dugan LL, Gabrielsen JK, Yu SP, Lin T-S, Choi DW. Buckminster fullerenol free radical scavengers reduce excitotoxic and apoptotic death of cultured cortical neurons. *Neurobiol Dis*. 1996;3(2):129–135.
134. Dugan LL, Turetsky DM, du C, et al. Carboxyfullerenes as neuroprotective agents. *Proc Natl Acad Sci U S A*. 1997;94(17):9434–9439.
135. Huang Y-L, Shen CK-F, Luh T-Y, Yang HC, Hwang KC, Chou C-K. Blockage of apoptotic signaling of transforming growth factor-beta in human hepatoma cells by carboxyfullerene. *Eur J Biochem*. 1998;254(1):38–43.
136. Tokuyama H, Yamago S, Nakamura E, Shiraki T, Sugiura Y. Photoinduced biochemical activity of fullerene carboxylic acid. *J Am Chem Soc*. 1993;115(17):7918–7919.
137. Jensen AW, Wilson SR, Schuster DI. Biological applications of fullerenes. *Bioorg Med Chem*. 1996;4(6):767–779.
138. Iwata N, Mukai T, Yamakoshi Y, et al. Effect of C_{60}, a fullerene, on the activities of glutathione *S*-transferase and glutathione-related enzymes. *Fullerene Sci Technol*. 1998;6:213–226.
139. Ueng TH, Kang JJ, Wang HW, Cheng YW, Chiang LY. Suppression of microsomal cytochrome P450-dependent monooxygenases and mitochondrial oxidative phosphorylation by fullerenol, a polyhydroxylated fullerene C60. *Toxicol Lett*. 1997;93(1):29–37.
140. Sijbesma R, Srdanov G, Wudl F, et al. Synthesis of a fullerene derivative for the inhibition of HIV enzymes. *J Am Chem Soc*. 1993;115(15):6510–6512.
141. Bosi S, da Ros T, Castellano S, Banfi E, Prato M. Antimycobacterial activity of ionic fullerene derivatives. *Bioorg Med Chem Lett*. 2000;10(10):1043–1045.
142. da Ros T, Prato M, Novello F, Maggini M, Banfi E. Easy access to water-soluble fullerene derivatives via 1,3-dipolar cycloadditions of azomethine ylides to C60. *J Org Chem*. 1996;61(25):9070–9072.
143. Mashino T, Okuda K, Hirota T, Hirobe M, Nagano T, Mochizuki M. Inhibition of *E. coli* growth by fullerene derivatives and inhibition mechanism. *Bioorg Med Chem Lett*. 1999;9(20):2959–2962.
144. Bianco A, da Ros T, Prato M, Toniolo C. Fullerene-based amino acids and peptides. *J Pept Sci*. 2001;7(4):208–219.
145. Bosi S, da Ros T, Spalluto G, Prato M. Fullerene derivatives: an attractive tool for biological applications. *Eur J Med Chem*. 2003;38(11–12):913–923.
146. Pantarotto D, Bianco A, Pellarini F, et al. Solid-phase synthesis of fullerene-peptides. *J Am Chem Soc*. 2002;124(42):12543–12549.
147. Orme MW, Labroo VM. Synthesis of β-estradiol-3-benzoate-17-(succinyl-12A-tetracycline): a potential bone-seeking estrogen. *Bioorg Med Chem Lett*. 1994;4(11):1375–1380.
148. Meyer JL, Nancollas GH. The influence of multidentate organic phosphonates on the crystal growth of hydroxyapatite. *Calcif Tissue Res*. 1973;13(1):295–303.
149. Willson TM, Charifson PS, Baxter AD, Geddie NG. Bone targeted drugs 1. Identification of heterocycles with hydroxyapatite affinity. *Bioorg Med Chem Lett*. 1996;6(9):1043–1046.
150. Gonzalez K, Wilson LJ, Wu W, Nancollas GH. Synthesis and in vitro characterization of a tissue-selective fullerene: vectoring C60(OH)16AMBP to mineralized bone. *Bioorg Med Chem*. 2002;10(6):1991–1997.
151. Shinohara H. Endohedral metallofullerenes. *Rep Prog Phys*. 2000;63(6):843–892.
152. Cagle DW, Kennel SJ, Mirzadeh S, Alford JM, Wilson LJ. In vivo studies of fullerene-based materials using endohedral metallofullerene radiotracers. *Proc Natl Acad Sci U S A*. 1999;96(9):5182–5187.
153. Cagle DW, Thrash TP, Alford M, Chibante LPF, Ehrhardt GJ, Wilson LJ. Synthesis, characterization, and neutron activation of holmium metallofullerenes. *J Am Chem Soc*. 1996;118(34):8043–8047.
154. Ping ZX, Qing Hua Z, Gao Qing L, Ai Bing Y. Inorganic nanoparticles as carriers for efficient cellular delivery. *Chem Eng Sci*. 2006;61:1027–1040.
155. Nakamura E, Isobe H, Tomita N, Sawamura M, Jinno S, Okayama H. Functionalized fullerene as an artificial vector for transfection. *Angew Chem Int Ed Engl*. 2000;39(23):4254–4257.
156. Foley S, Crowley C, Smaihi M, et al. Cellular localisation of a water-soluble fullerene derivative. *Biochem Biophys Res Commun*. 2002;294(1):116–119.
157. Yamago S, Tokuyama H, Nakamura E, et al. In vivo biological behavior of a water-miscible fullerene: 14C labeling, absorption, distribution, excretion and acute toxicity. *Chem Biol*. 1995;2(6):385–389.
158. Mcneil SE. Nanotechnology for the biologist. *J Leukoc Biol*. 2005;78(3):585–594.
159. Sun C, Lee J, Zhang M. Magnetic nanoparticles in MR imaging and drug delivery. *Adv Drug Deliv Rev*. 2008;60(11):1252–1265.
160. Echegoyen L, Echegoyen LE. Electrochemistry of fullerenes and their derivatives. *Acc Chem Res*. 1998;31(9):593–601.
161. Wickline SA, Neubauer AM, Winter PM, Caruthers SD, Lanza GM. Molecular imaging and therapy of atherosclerosis with targeted nanoparticles. *J Magnet Reson Imaging*. 2007;25(4):667–680.
162. Ito A, Shinkai M, Honda H, Kobayashi T. Medical application of functionalized magnetic nanoparticles. *J Biosci Bioeng*. 2005;100(1):1–11.
163. Wetzler M, Thomas DA, Wang ES, et al. Phase I/II trial of nanomolecular liposomal annamycin in adult patients with relapsed/refractory acute lymphoblastic leukemia. *Clin Lymphoma Myeloma Leuk*. 2013;13(4):430–434.
164. Long Q, Xie Y, Huang Y, et al. Induction of apoptosis and inhibition of angiogenesis by PEGylated liposomal quercetin in both cisplatin-sensitive and cisplatin-resistant ovarian cancers. *J Biomed Nanotechnol*. 2013;9(6):965–975.
165. Zhou J, Zhao W-Y, Ma X, et al. The anticancer efficacy of paclitaxel liposomes modified with mitochondrial targeting conjugate in resistant lung cancer. *Biomaterials*. 2013;34(14):3626–3638.
166. Wang J, Peng CA. Anticancer effectiveness of polymeric drug nanocarriers on colorectal cancer cells. *Conf Proc IEEE Eng Med Biol Soc*. 2011;1:3249–3252.
167. Li Y, Jin M, Shao S, et al. Small-sized polymeric micelles incorporating docetaxel suppress distant metastases in the clinically-relevant 4T1 mouse breast cancer model. *BMC Cancer*. 2014;14(1):329.

168. Chen L, Sha X, Jiang X, Chen Y, Ren Q, Fang X. Pluronic P105/F127 mixed micelles for the delivery of docetaxel against taxol-resistant non-small cell lung cancer: optimization and in vitro, in vivo evaluation. *Int J Nanomedicine*. 2013;8:73–84.
169. Weiss GJ, Chao J, Neidhart JD, et al. First-in-human Phase 1/2a trial of CRLX101, a cyclodextrin-containing polymer-camptothecin nanopharmaceutical in patients with advanced solid tumor malignancies. *Invest New Drugs*. 2013;31(4):986–1000.
170. Yellepeddi V, Kumar A, Palakurthi S. Biotinylated poly(amido)amine (PAMAM) dendrimers as carriers for drug delivery to ovarian cancer cells in vitro. *Anticancer Res*. 2009;29(8):2933–2943.
171. Kukowska-Latallo JF, Candido KA, Cao Z, et al. Nanoparticle targeting of anticancer drug improves therapeutic response in animal model of human epithelial cancer. *Cancer Res*. 2005;65(12):5317–5324.
172. Kolhe P, Misra E, Kannan RM, Kannan S, Lieh-Lai M. Drug complexation, in vitro release and cellular entry of dendrimers and hyperbranched polymers. *Int J Pharm*. 2003;259(1–2):143–160.
173. Hampel S, Kunze D, Haase D, et al. Carbon nanotubes filled with a chemotherapeutic agent: a nanocarrier mediates inhibition of tumor cell growth. *Nanomedicine*. 2008;3(2):175–182.
174. Hadjikirova M, Troyanova P, Simeonova M. Nanoparticles as drug carrier system of 5-fluorouracil in local treatment of patients with superficial basal cell carcinoma. *J BUON*. 2005;10(4):517.
175. Ringel J, Erdmann K, Hampel S, et al. Carbon nanofibers and carbon nanotubes sensitize prostate and bladder cancer cells to platinum-based chemotherapeutics. *J Biomed Nanotechnol*. 2014;10(3):463–477.
176. Muthukumar T, Prabhavathi S, Chamundeeswari M, Sastry TP. Biomodified carbon nanoparticles loaded with methotrexate Possible carrier for anticancer drug delivery. *Mater Sci Eng C Mater Biol Appl*. 2014;36(36):14–19.
177. Ali-Boucetta H, Al-Jamal KT, Mccarthy D, et al. Multiwalled carbon nanotube–doxorubicin supramolecular complexes for cancer therapeutics. *Chem Commun (Camb)*. 2008;2(4):459–461.
178. Kumar A, Huo S, Zhang X, et al. Neuropilin-1-targeted gold nanoparticles enhance therapeutic efficacy of platinum(IV) drug for prostate cancer treatment. *ACS Nano*. 2014;8(5):4205–4220.
179. Sánchez-Paradinas S, Pérez-Andrés M, Almendral-Parra MJ, et al. Enhanced cytotoxic activity of bile acid cisplatin derivatives by conjugation with gold nanoparticles. *J Inorg Biochem*. 2014;131:8–11.
180. Chen Y-H, Tsai C-Y, Huang P-Y, et al. Methotrexate conjugated to gold nanoparticles inhibits tumor growth in a syngeneic lung tumor model. *Mol Pharm*. 2007;4(5):713–722.
181. Benezra M, Penate-Medina O, Zanzonico PB, et al. Multimodal silica nanoparticles are effective cancer-targeted probes in a model of human melanoma. *J Clin Invest*. 2011;121(7):2768–2780.
182. Xi D, Dong S, Meng X, et al. Gold nanoparticles as computerized tomography (CT) contrast agents. *RSC Adv*. 2012;2(33):12515–12524.
183. Kloepfer JA, Mielke RE, Wong MS, et al. Quantum dots as strain- and metabolism-specific microbiological labels. *Appl Environ Microbiol*. 2003;69(7):4205–4213.
184. Wang YX. Superparamagnetic iron oxide based MRI contrast agents: current status of clinical application. *Quant Imaging Med Surg*. 2011;1:35–40.
185. Miller L, Winter G, Baur B, et al. Synthesis, characterization, and biodistribution of multiple ^{89}Zr-labeled pore-expanded mesoporous silica nanoparticles for PET. *Nanoscale*. 2014;6(9):4928–4935.
186. Jain TK, Richey J, Strand M, Leslie-Pelecky DL, Flask CA, Labhasetwar V. Magnetic nanoparticles with dual functional properties: drug delivery and magnetic resonance imaging. *Biomaterials*. 2008;29(29):4012–4021.
187. Zerda A, Liu Z, Bodapati S, et al. Ultrahigh sensitivity carbon nanotube agents for photoacoustic molecular imaging in living mice. *Nano Lett*. 2010;10(6):2168–2172.
188. Hirsch LR, Stafford RJ, Bankson JA, et al. Nanoshell-mediated near-infrared thermal therapy of tumors under magnetic resonance guidance. *Proc Natl Acad Sci U S A*. 2003;100(23):13549–13554.
189. Ismail AF, Ali MM, Ismail LF. Photodynamic therapy mediated antiproliferative activity of some metal-doped ZnO nanoparticles in human liver adenocarcinoma HepG2 cells under UV irradiation. *J Photochem Photobiol B*. 2014;138C:99–108.
190. Nurunnabi M, Khatun Z, Reeck GR, et al. Photoluminescent graphene nanoparticles for cancer photo-therapy and imaging. *ACS Appl Mater Interfaces*. 2014;6(15):12413–12421.
191. Li Z, Pan LL, Zhang FL, Wang Z, Shen YY, Zhang ZZ. Preparation and characterization of fullerene (C_{60}) amino acid nanoparticles for liver cancer cell treatment. *J Nanosci Nanotechnol*. 2014;14(6):4513–4518.
192. Johannsen M, Jordan A, Scholz R, et al. Evaluation of magnetic fluid hyperthermia in a standard rat model of prostate cancer. *J Endourol*. 2004;18(5):495–500.
193. Jordan A, Scholz R, Maier-Hauff K, et al. The effect of thermotherapy using magnetic nanoparticles on rat malignant glioma. *J Neurooncol*. 2006;78(1):7–14.
194. Huang X, Jain PK, El-Sayed IH, El-Sayed MA. Plasmonic photothermal therapy (PPTT) using gold nanoparticles. *Lasers Med Sci*. 2008;23(3):217–228.
195. Mackey MA, Ali MR, Austin LA, Near RD, El-Sayed MA. The most effective gold nanorod size for plasmonic photothermal therapy: theory and *in* vitro experiments. *J Phys Chem B*. 2014;118(5):1319–1326.
196. Marches R, Mikoryak C, Wang RH, Pantano P, Draper RK, Vitetta ES. The importance of cellular internalization of antibody-targeted carbon nanotubes in the photothermal ablation of breast cancer cells. *Nanotechnology*. 2011;22(9):095101.
197. Wang CH, Huang YJ, Chang CW, Hsu WM, Peng CA. *In vitro* photothermal destruction of neuroblastoma cells using carbon nanotubes conjugated with GD2 monoclonal antibody. *Nanotechnology*. 2009;20(31):315101.
198. Oishi M, Nakaogami J, Ishii T, Nagasaki Y. Smart PEGylated gold nanoparticles for the cytoplasmic delivery of siRNA to induce enhanced gene silencing. *Chem Lett*. 2006;35(9):1046–1047.
199. Terranova ML, Sessa V, Rossi M. The world of carbon nanotubes: an overview of CVD growth methodologies. *Chem Vapor Depos*. 2006;12(6):315–325.
200. Tripisciano C, Kraemer K, Taylor A, Borowiak-Palen E. Single-wall carbon nanotubes based anticancer drug delivery system. *Chem Phys Lett*. 2009;478(4-6):200–205.
201. Wu W, Li R, Bian X, et al. Covalently combining carbon nanotubes with anticancer agent: preparation and antitumor activity. *ACS Nano*. 2009;3(9):2740–2750.
202. Ali-Boucetta H, Al-Jamal KT, Mccarthy D, Prato M, Bianco A, Kostarelos K. Multiwalled carbon nanotube–doxorubicin supramolecular complexes for cancer therapeutics. *Chem Commun (Camb)*. 2008;4:459–461.
203. Liu Z, Tabakman S, Welsher K, Dai H. Carbon nanotubes in biology and medicine: in vitro and in vivo detection, imaging and drug delivery. *Nano Res*. 2009;2(2):85–120.
204. Barone PW, Baik S, Heller DA, Strano MS. Near-infrared optical sensors based on single-walled carbon nanotubes. *Nat Mater*. 2005;4(1):86–92.
205. Grabowska J. Fulereny – przyszłość zastosowań w medycynie i farmacji. *Gaz Farm*. 2008;6:38–40.
206. Ionut IA, Tiperciuc B, Oniga O, Szefler B, Maties R. Correlating study on phisyco-chemical and biological properties of thiosemicarbazone and thiadiazoline derivatives. *Stud Univ Babes-Bolyai Chem*. 2012;57(3):109–119.
207. Maties R, Szefler B, Ionut I, Tiperciuc B. QSPR study on the chromatographic behaviour of a set of thiazole derivatives by autocorrelation analysis. *Stud Univ Babes-Bolyai Chem*. 2012;57(4):121–133.
208. Harsa TE, Harsa AM, Szefler B. QSAR of caffeines by similarity cluster prediction. *Cent Eur J Chem*. 2014;12(3):365–376.
209. Maties R, Szefler B, Diudea MV. QSAR study on dioxins. *Stud Univ Babes-Bolyai Chem*. 2015;60(4):193–200.

210. Harsa TE, Harsa AM, Diudea MV, Szefler B. QSAR and docking studies of dopamine derivatives by similarity cluster prediction. *Rev Roum Chim*. 2015;60(7–8):727–733.
211. Chen Z, Ma L, Liu Y, Chen C. Applications of functionalized fullerenes in tumor theranostics. *Theranostics*. 2012;2(3):238–250.
212. Szefler B, Harsa TE, Harsa AM. QSAR and docking study on Indolizines by similarity clustering. *Stud Univ Babes-Bolyai Chem*. 2015; 60(4):201–212.
213. Harsa TE, Harsa AM, Szefler B, Diudea MV. QSAR study on caffeine derivatives docked on poly(A)RNA polymerase protein cid1. *Croat Chem Acta*. 2016;89(1):17–24.
214. Lungu C, Ersali S, Szefler B, Pîrvan-Moldovan A, Basak S, Diudea MV. Dimensionality of big data sets explored by Cluj descriptors. *Stud Univ Babes-Bolyai Chem*. 2017;62(3):197–204.
215. Czeleń P, Szefler B. Molecular dynamics study of ChEMBL474807 inhibition properties against GSK3 and CDK2 enzymes. *J Mol Model*. 2015;21(4):1–8.
216. Szefler B, Diudea MV, Grudziński IP. Nature of polyethyleneimine–glucose oxidase interactions. *Stud Univ Babes-Bolyai Chem*. 2016; 61:249–260.
217. Szefler B, Diudea MV, Putz MV, Grudziński IP. Molecular dynamic studies of the complex polyethylenimine and glucose oxidase. *Int J Mol Sci*. 2016;17(11)pii:E1796.
218. Szefler B, Czeleń P, Diudea MV. Understanding the action of indolizines as biologically active moieties: a molecular dynamics study. *Curr Comput Aided Drug Des*. 2017;13(1):22–29.
219. Szefler B, Czeleń P. Potential inhibitory effect of indolizine derivatives on the two enzymes: nicotinamide phosphoribosyltransferase and beta lactamase, a molecular dynamics study. *J Mol Model*. 2017; 23(7):208.
220. RCSB PDB, GOx – molecule of the month, May 2006. Available from: https://pdb101.rcsb.org/motm/77. Accessed September 21, 2018.
221. Wiśniewski M, Rossochacka P, Werengowska-Ciećwierz K, et al. Medyczne aspekty nanostrukturalnych materiałów węglowych. *Inż Ochr Środow* [Medical aspects of nanostructured carbon materials]. 2013;16(2):255–261. Polish.
222. Justyna Żwawiak J, Katarzyna Sowa-Kasprzak K. Nanocząstki w roli nośników substancji aktywnych. Nanoparticles as carriers of active substances. Farm Współ. 2014;7:175–182.
223. Hygeia Public Health. 2014;49(3):449–457.
224. Wan F. Introduction to the Calculus of Variations and its Applications. Routledge, 2017.